Universidade de São Paulo
Instituto de Física

A influência do Líquido lônico $[C_{14}MIM][Cl]$ nas características estruturais e termodinâmicas de membranas modelos zwiterionicas e ânionicas.

Luma Melo de Oliveira

Orientador: Prof. Dr. Leandro R. S. Barbosa

Dissertação de mestrado apresentada ao Instituto de Física para a obtenção do título de Mestre em Ciências

Banca Examinadora:
Dr. Leandro R. S. Barbosa (IF-USP)
Profa. Dra. Carlota de Oliveira Rangel-Yagui (FCF -USP)
Prof. Dr. Luciano Caseli (UNIFESP)

São Paulo
2017

FICHA CATALOGRÁFICA
Preparada pelo Serviço de Biblioteca e Informação
do Instituto de Física da Universidade de São Paulo

Oliveira, Luma Melo de

A influência do líquido iônico [C14MIM][Cl] nas características estruturais e termodinâmicas de membranas modelos zwiterionicas e aniônicas. São Paulo, 2017.

Dissertação (Mestrado) – Universidade de São Paulo. Instituto de Física. Depto. de Física Geral

Orientador: Prof. Dr. Leandro Ramos Souza Barbosa

Área de Concentração: Biofísica

Unitermos: 1. Biofisica; 2. Lipídeos; 3. Líquidos iônicos; 4. SAXS.

USP/IF/SBI-023/2017

Universidade de São Paulo
Instituto de Física

The influence of the Ionic Liquid $[C_{14}MIM][Cl]$ on the structural and thermodynamic features of zwitterionic and anionic model membrane

Luma Melo de Oliveira

Advisor: Prof. Dr. Leandro R. S. Barbosa

Master thesis presented to the Institute of Physics for obtaining a Master's degree in science

Banca Examinadora:
Dr. Leandro R. S. Barbosa (IF-USP)
Profa. Dra. Carlota de Oliveira Rangel-Yagui (FCF -USP)
Prof. Dr. Luciano Caseli (UNIFESP)

São Paulo
2017

I dedicate this thesis to my best friend Victor Santoro Fernandes so he never forgets.

Você deve notar que não tem mais tutu
e dizer que não está preocupado
Você deve lutar pela xepa da feira
e dizer que está recompensado
Você deve estampar sempre um ar de alegria
e dizer: tudo tem melhorado
Você deve rezar pelo bem do patrão
e esquecer que está desempregado

Você merece, você merece
Tudo vai bem, tudo legal
Cerveja, samba, e amanhã, seu Zé
Se acabarem com o teu Carnaval?

Você deve aprender a baixar a cabeça
E dizer sempre: "Muito obrigado"
São palavras que ainda te deixam dizer
Por ser homem bem disciplinado
Deve pois só fazer pelo bem da Nação
Tudo aquilo que for ordenado
Pra ganhar um Fuscão no juízo final
E diploma de bem comportado

Tudo vai bem, tudo legal

Luiz Gonzaga Jr., Gonzaguinha.

Acknowledgments

Firstly, I would like to express my sincere gratitude to my advisor Prof. Dr, Leandro R. S. Barbosa for the continuous support on my master study and related research, for his patience, motivation, and immense knowledge.

Besides my advisor, I would like to thank Prof[a]. Dr[a]. Rosangela Itri for her insightful comments, encouragement and stimulus to widen my research from various perspectives.

A special thanks to Prof[a]. Dr[a] Denise Petri; the National Laboratory of Synchrotron Light (LNLS); and the Biophysics Laboratory (IF-USP) for providing me access to their laboratories and research facilities.

I thank my fellow lab mates. In particular, I am grateful to MSc Juliana Raw, MSc Gustavo Scanavachi and Rafaella de Rosa for the stimulating discussions, help and for all the fun we have had in the last two years.

Gratitude to Najla and Luthi for helping me when I most needed. I will always be grateful.

To my sister, best friend, mother, father, guide and so forth, Luana. Thank you for teaching me everything you know and pushing me forward. My bravery is consequence of your love.

To Victor Santoro Fernandes to whom I dedicated my 2-years-work of this thesis. Thanks for not letting me boycott myself and soften the chaos of life. “Algo além do Sol me esquenta”

To Tahira and Dinis for being my life partners, with whom I grow old together. What we have no one can imagine. Thanks for loving me for who I am.

To Natasha Magid and Juliana for helping keep me sane and happy.

To all my dearest and craziest friends Vinicius Martins, Carlos Flanga, Daniel Pamio, Lucas Vale, Julianna Testoni, Bruna Carvalho, Roxana Cabrera, Luiz Mira, Nádia Gregório and Nathália Gaguetti.

To my team colleagues of BAFEFI, Amélia Império Rugby and Tsunami. Keep playing like girls.

Last but not the least, I would like to thank my parents for supporting me throughout my life in general.

Acknowledgements to Capes for the financial support.

Resumo

Os líquidos iônicos (LI) tem atraído grande atenção, tanto da academia quanto da indústria, devido às suas numerosas aplicações. LI são sais, normalmente compostos por um íon orgânico, e um contra-íon que pode ser orgânico ou inorgânico, mas que tem como característica ser encontrado no estado líquido à temperaturas próximas a ambiente. Nosso interesse em estudar LIs vem de sua baixa toxicidade, atribuída a sua baixa volatilidade. Entretanto, alguns estudos recentes mostraram que a toxicidade dos LI é maior do que se acreditava, em particular com sistemas de relevância biológica. O objetivo principal desta dissertação é estudar a influência do líquido iônico 1-tetradecil-3-metilimidazólio cloreto ([C_{14}MIM][Cl]) com sistemas de membrana. Para isso, utilizamos diferentes lipídios, como o POPC, esfingomielina, colesterol, POPG, DPPC, DPPG e o DMPC. Para cada um destes sistemas, a influência da concentração de LI foi elucidada por meio de um estudo sistemático através de diferentes técnicas experimentais, tais como: espalhamento de raio-X a baixos ângulos (SAXS), espalhamento dinâmico de luz (DLS), anisotropia de fluorescência, microscopia óptica e potencial-ζ. Uma vez que o componente iônico de [C_{14}MIM][Cl] tem uma carga positiva no grupo imidazólio, a carga superficial de todas as vesículas estudadas aqui aumentou. Entretanto, para as vesículas compostas pelos lipídeos zwitteriónicos, não tenha sido observada qualquer alteração significativa no tamanho e na temperatura de transição de fase gel-fluido. O [C_{14}MIM][Cl] altera a organização interna entre as moléculas de lipídio com carga negativa. Consequentemente, à medida que a quantidade de LI aumenta, a temperatura de transição de fase diminui e o tamanho médio das vesículas aumenta. Para o sistema DPPC:DPPG (1:1) a temperatura de transição de fase caiu de 42.50 ± 0.13 ^{o}C para 25.27 ± 0.33 ^{o}C e para as vesículas de DPPG de 46.12±0.22 ^{o}C para 36.6±0.38 ^{o}C. Quanto ao diâmetro hidrodinâmico médio, no caso do DPPG este valor aumentou de 84±0.1 nm para 176±0.1 nm, enquanto que para a mistura DPPC:DPPG (1:1) ele passou de 95±0.1nm para 196±0.1nm. Indicando assim que o LI incorpora na bicamada lipídica negativamente carregada. O perfil de densidade eletrônica, obtido por SAXS, confirma a penetração do [C_{14}MIM][Cl] na bicamada lipídica. Diferentemente, para a membrana lipídica zwitteriónica o LI tende a se situar perto da região da cabeça polar sem afetar significativamente a região do interior da bicamada lipídica. Por outro lado, a presença de15 mol% de [C_{14}MIM][Cl] aumenta a espessura da região polar das bicamadas das vesículas de DPPC de ~ 11.1±0.6 Å para ~ 18.0±0.7 Å. Os resultados qualitativos da microscopia óptica mostraram que a incorporação da LI desestabiliza a assimetria da membrana entre as camadas interna e externa, além de sugerir o aparecimento de poros (evidenciado pela perda do contraste ótico das vesículas) e estruturas chamadas de buds. Esperamos que este trabalho melhore a compreensão dos efeitos do LI na presença de organismos biológicos.

Palavras-chave: lipídios, liquidos iônicos, membranas modelo, tensão superficial, DLS, potencial zeta, anisotropia de fluorescência, SAXS, microscopia ótica.

Abstract

Ionic Liquids (ILs) has been attracting attention, both from academia and industry, given the numerous applications of these systems. ILs are salts, usually composed by an organic ion, and a counterion which could be organic or inorganic, and, interestingly they are found at liquid state at room temperature. Our interest in studying ILs comes from its low toxicity. Some recent studies have shown that the toxicity of the ILs is higher than believed, in particular for biologically relevant systems. The main goal of this research is to study the influence of the ionic liquid 1-tetradecyl-3-methylimidazolium chloride ([C_{14}MIM][Cl]) with membrane systems. To do so, we made use of different lipids: POPC, Sphingomyelin, Cholesterol, POPG, DPPC, DPPG and DMPC. For each of these systems, the influence of ILs concentration were elucidated by means of a systematic study through different experimental techniques: Small Angle X-ray scattering (SAXS), dynamic light scattering (DLS), fluorescence anisotropy, optical microscopy and ζ-potential. Since [C_{14}MIM][Cl] has a positive charge on the imidazolium group, the superficial charge of all vesicles increased. For zwitterionic vesicles no significant change in size and melting temperature were noticed. The imidazolium-based ionic liquid diminished the gel-fluid transition temperature for negatively charged lipids. For DPPC:DPPG (1:1), for instance, the transition temperature decreased from 42.50±0.13^{o}C to 25.27±0.33^{o}C and for DPPG from 46.12±0.22 ^{o}C to 36.6±0.38 ^{o}C. For DPPG, the vesicle hydrodynamic diameter increased from 84±0.1nm to 176±0.1nm, whereas for DPPC:DPPG it increased from 95±0.1nm to 196±0.1nm. The electronic density profile, obtained by SAXS, supported the penetration of the [C_{14}MIM][Cl] into the negative bilayer structure. 15 mol% of *[C_{14}MIM][Cl] increased the polar head thickness of DPPC vesicles from 11.1±0.6 Å to 18.0±0.7 Å, without alter significantly the inner region of the membrane. Qualitative results obtained with optical microscopy showed that the IL incorporation destabilize the membrane asymmetry (between the leaflets) leading to the formation of pores (evidenced by optical contrast lost) and the presence of bud's. We believe that this work could improve the understanding of the effects of ILs in the presence of biological relevant systems.*

Key words: lipids, ionic liquids, model membranes, surface tension, DLS, zeta potential, fluorescence anisotropy, SAXS, optical microscopy

Contents

Contents

List of abbreviations

[C_{14}MIM][Cl] - 1-tetradecyl-3-methylimidazolium chloride

CMC - Critical Micellar Concentration

DLS - Dynamic Light Scattering

DMPC - 1,2-dimyristoyl-sn-glyecro-3-phosphatidylcholine

DPH - 1,6-Diphenyl-1,3,5-hexatriene

DPPC - 1,2-dipalmitoyl-sn-glyecro-3-phosphatidylcholine

DPPG - 1,2-dipalmitoyl-sn-glyecro-3-phosphatidylglycerol

DSC - Differential Scattering Calorimetry

GUV - Giant Unilamellar Vesicles

HPLC - High performance liquid chromatography or high pressure liquid chromatography

IL - Ionic Liquids

ITO - Indium Tin Oxide

IUPAC – International Union of Pure and Applied Chemistry

LNLS - Laboratório Nacional de Luz Sincrotron

LUV - Large Unilamellar Vesicles

PdI - Polydispersity Index

POPC - 1-palmitoyl-2-oleoyl-sn-glyecro-3-phosphatidylcholine

POPG - 1-palmitoyl-2-oleoyl-sn-glyecro-3-phosphatidylglycerol

RICM - Reflection Interference Contrast Microscopy

SAXS - Small Angle X-Ray Scattering

SDS - Sodium dodecyl sulfate

SM - Sphingomyelin

Ch - Cholesterol

1. Introduction

The Green Chemistry is defined by IUPAC (*International Union of Pure and Applied Chemistry*) as: *"The invention, development and application of products and chemical processes to reduce or eliminate the generation and use of dangerous substances"* (TUNDO et al., 2000). In this context, one of the most active subareas of Green Chemistry is the solvent research (ANASTAS; KIRCHHOFF, 2002; DESIMONE, 2002; LI; TROST, 2008), in which we find the Ionic Liquids (IL) as one of the key-featured solvents. In the last decade, more than 17300 papers were published containing "ionic liquids" in the title[1], due to its interesting physical and chemical properties, like their nonvolatile nature, which empowers significantly engineering applications, and their ability in being at the liquid state at temperatures < 100^{o}C, for instance (ZHENG et al., 2013).

The importance of IL as ecological solvents made its interaction with biologically relevant systems more attractive. However, assure that IL has a low biological impact is not accurate. So, its interaction with liposomes (GAL et al., 2012; PATRA et al., 2012) and proteins (VENTURA et al., 2011, 2012) are being more and more investigated in the last few years. Despite the large amount of research dealing with the interaction of alky-functionalized IL with biomimetic systems (GAL et al., 2012), the specific interaction of IL on the membrane structural features remains unclear. Firstly, we show a briefly introduction regarding the ionic liquids properties as well as the phospholipids that were used in the present study.

[1] Research done on Google Scholar in February 2nd, 2017.

1.1 Ionic Liquids

Ionic liquids are unconventional salts, which because of their complex chemical structure, are at the liquid state at temperatures smaller than 100^{o}C, including room temperature range (ENDRES et al., 2010). The anion and cation are chosen precisely to destabilize the solid-phase (PAUL; MOULIK, 2015), disfavoring the crystallization processes and, as a consequence, inducing the liquid state. While there are no set rules to synthetize ILs, in general, this can be achieved within a relatively large window of ionic structures by balancing ion−ion interactions (HAYES et al., 2012; WASSERSCHEID; KEIM, 2000).

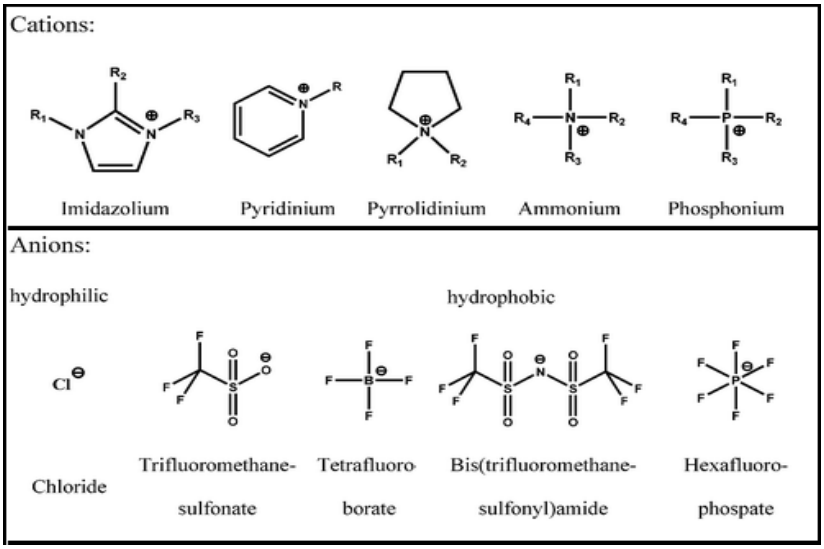

Figure 1.1: Cations and anions common examples in IL structures. Source: (ERDMENGER et al., 2010)

For instance, diversity of anions and cations leads to a varied physicochemical intriguing properties, like the already mentioned low melting point (<100ºC) (CHIAPPE; PIERACCINI, 2005; HAYES et al., 2012; POLESKI et al., 2013), high capacity of solubility in water (BERTHOD; RUIZ-ÁNGEL; CARDA-BROCH, 2008; CARDA-BROCH; BERTHOD; ARMSTRONG, 2003; CHIAPPE; PIERACCINI, 2005), low vapor pressure (BERTHOD; RUIZ-ÁNGEL; CARDA-

BROCH, 2008; CARDA-BROCH; BERTHOD; ARMSTRONG, 2003) and high conductivity (due to its ionic nature) (CARDA-BROCH; BERTHOD; ARMSTRONG, 2003; CHIAPPE; PIERACCINI, 2005; HAYES et al., 2012). Besides, they can be functionalized by associating with one or more acyl chains (YU; HO; ANDERSON, 2013), which confer a surfactant-like behavior to the IL (HAYES et al., 2012; TUNDO et al., 2000; YANG; PAN, 2005). Some of these common cations and anions are showed in Figure 1.1.

GAL et al. (GAL et al., 2012) revealed that ILs functionalized with longer acyl chains (n > 7, being *n* the number of methylene groups in the acyl chain) exhibit a surfactant-like behavior, including micelles formation above a specific concentration, the critical micellar concentration (CMC). Moreover, Jeong et al. (JEONG et al., 2012) also demonstrated that IL can incorporate into DMPC membranes, depending on the acyl chains length. Long chain IL can penetrate into the vesicle, inducing disorder and rapidly disrupting and destroying it (JEONG et al., 2012).

In such manner, the IL employed in this work was chosen due to its large acyl chains and similarity, in structure, with the hydrophobic portion of the lipids, i.e., the long acyl chain. Chart 1.1 shows the chemical structure of $[C_{14}MIM][Cl]$, the IL employed in this study.

Name	Number of methylene groups	Structure
1-tetradecyl-3-methylimidazolium chloride	14	$[C_{14}MIM][Cl]$ 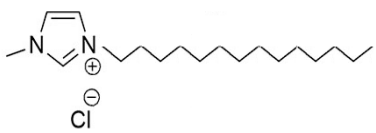

Chart 1.1 : Ionic Liquid employed in this work. In first column the name, in the second the number of methylene groups and in the last one the chemical structure.

The chosen IL have an imidazolium ring as the cationic component of the salt. It is also functionalized with an acyl chain 14-methylene groups-long and the counter-ion is the chloride (Cl^-) (Chart 1.1).

1.2 Phospholipids

Phospholipids are amphiphilic molecules with hydrophilic region named polar head group and a hydrophobic region, generally composed by acyl chains (PATRA et al., 2012). They are the major component of cellular membranes, can form a large variety of known structures and are present in several organelles, like mitochondrion, for instance (BLUME, 1993).

Noteworthy, in the cellular environment, i.e., *in natura* the cellular membrane is not a simple structure. In other words, it can be formed by more than 200 different kinds of phospholipids (LEHNINGER, 1993). In order to simplify such problem, it is common to use a “synthetic” system to simulate cellular membranes. Such a simplification can help the understand of molecular mechanisms in cell and organelles. Regarding its amphiphilic behavior, the polar head groups can be negatively charged (anionic phospholipids) or possess both negative and positive charge, acquiring then an electric dipole (zwitterionic phospholipids). Moreover, the phospholipid may exhibit structural differences in their hydrophobic tail by the number of methylene groups and the absence or presence of unsaturation along the acyl chain (BLUME, 1993; CEVC; MARSH, 1987).

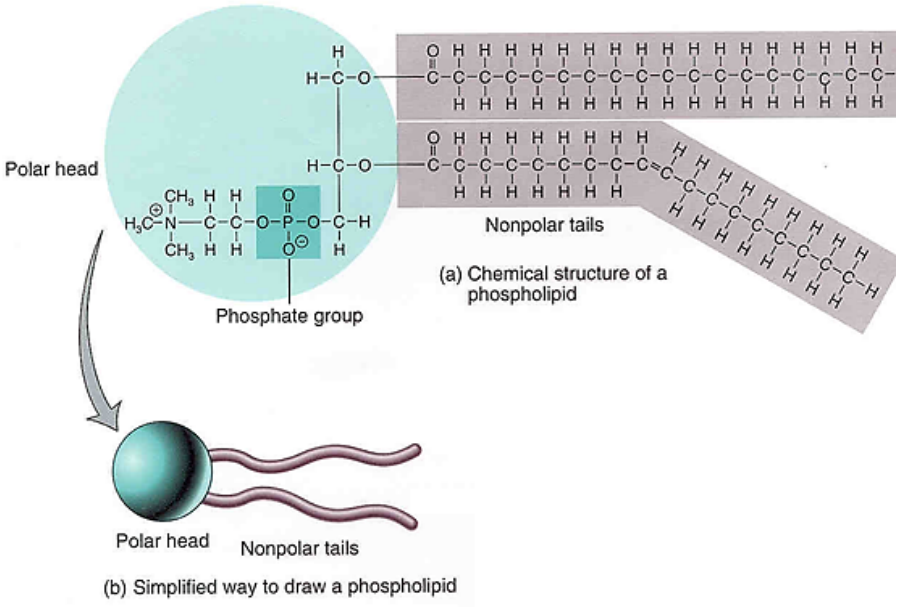

Figure 1.2: Phospholipid structure. (a) Chemical structure (b) Simplified sketch of a general phospholipid. Source: http://homepage.smc.edu/wissmann_paul/anatomy2textbook/phospholipid.jpg

In solution, the water (polar solvent) tries to to maximize contact with the hydrophilic region, while the opposite happens for the hydrophobic portion of the molecule. The acyl chain cannot interact with water by hydrogen bond, because of that, the energy to keep lipids in solution is higher (Figure 1.2 A), thus water is able to assemble the phospholipids and minimizes the contact with the acyl chains , favoring the self-assemble process. (Figure 1.2 B)

At relatively low concentrations, the molecules in solution are mostly at the air-water interface (Figure 1.2 A). At relatively high concentrations, however, the molecules tend to organize themselves in order to minimize contact with water molecules (Figure 1.2 B).

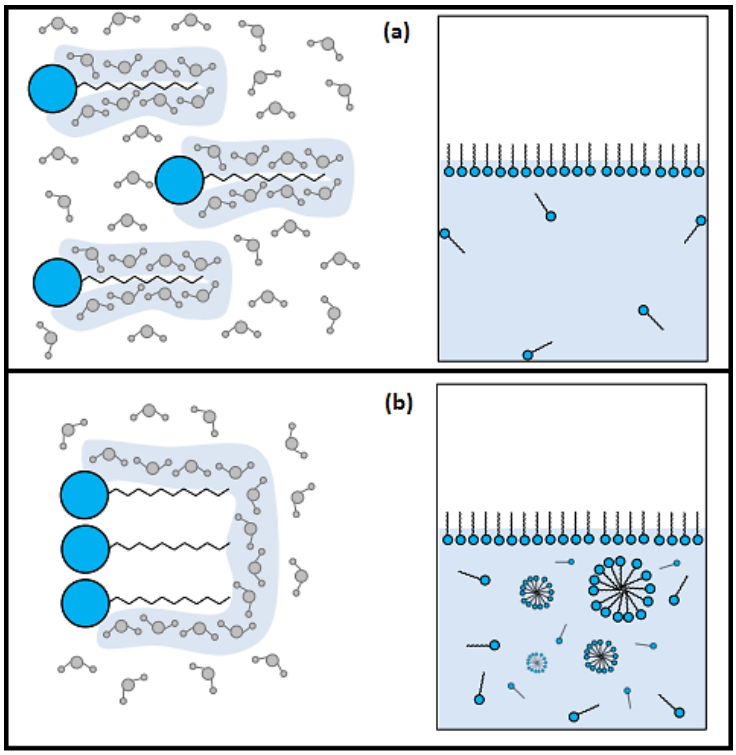

Figure 1.3: Hydrophobic effect representation. In (a) the molecule is in the interface and in (b) the molecules self-assemble in micelles. Adapted from (BOYLE, 2005; FILHO, 2013)

There is a specific concentration value that above, molecules self-assemble into micelles, or other aggregates. This concentration is called *critical micelle concentration* (CMC). This particular concentration depends on several intrinsic factor, e.g., the hydrophobic region size, the molecular volume of both hydrophobic and hydrophilic regions, pH, ionic strength, temperature, among others (DOMÍNGUEZ et al., 1997) (ISRAELACHVILI, 1991).

The self-assembled structures depend on the geometry of the molecule. This dependence is given by the adimensional *packing factor p* defined as (ISRAELACHVILI, 1991):

$$p = \frac{V_T}{A_H l_T} \qquad \textbf{(1. 1)}$$

where V_T is the volume of the hydrophobic region, A_H the polar region cross-section area and l_T the length of the acyl chain (BLUME, 1993). In Figure 1.4, the packing factors, *p*, of some structures are shown(ISRAELACHVILI, 1991).

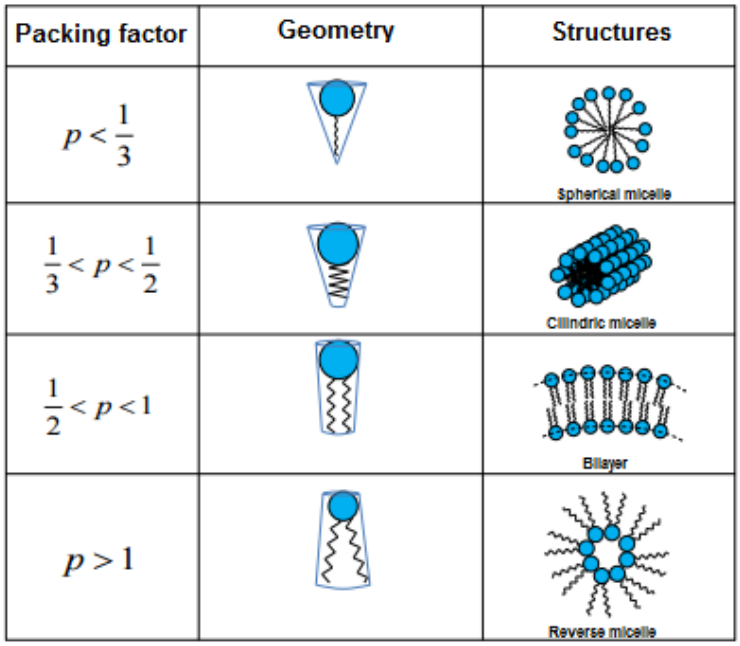

Figure 1.4: Packing factor of some of the most common structures. Adapted from (ISRAELACHVILI, 1991)

The phospholipids used in this work self-assemble into bilayer to create liposomes (BLUME, 1993) due to its cylindrical geometry. Noteworthy, Figure 1.5 shows a schematic representation of the liposomes, the relative size of the inner water-containing region as well as the bilayer thickness are not in scale.

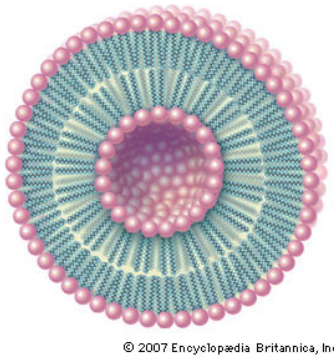

Figure 1.5: Liposome model. Source: (ENCYCLOPEDIA BRITANNICA, 2010)

Liposomes are classified by multilamellar vesicle (MLV, with several stacked bilayers separated by a small water layer) and unilamellar vesicles. Into the unilamellar vesicles, it is categorized by its external diameter: SUVs (Small Unilamellar Vesicles, smaller than 100nm), LUVs (Large Unilamellar Vesicles that range typically from 100-500nm) and GUVs (Giant Unilamellar Vesicles with diameter > 1-100 μm) (STRYER, 1981). In the present study, we focused our attention into LUVs and GUVs. Their preparation methods are different and it will be described later on in Chapter 2.

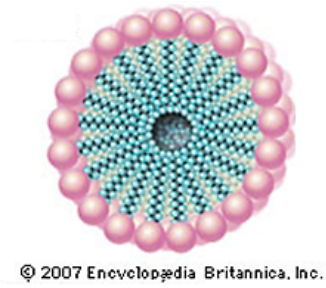

Figure 1.6: Micelle model. Source: (ENCYCLOPEDIA BRITANNICA, 2010)

Interestingly, ILs, due to its molecular structure, self-assemble into micelles (Figure 1.6). Besides phospholipids, there is another type of lipid called sphingolipids that have the same behavior as the phospholipids when in aqueous solution (PERETÓ et al., 2007). All structures of the six different phospholipids and the sphingolipid used in this thesis are presented in Table 1. 1.

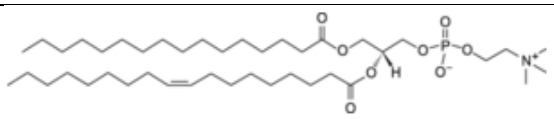	Palmitoyl phosphatidylcholine **(POPC)**
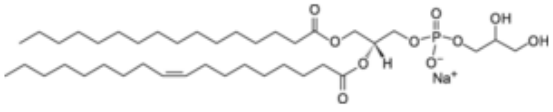	Palmitoyl phosphatidyl glycerol **(POPG)**

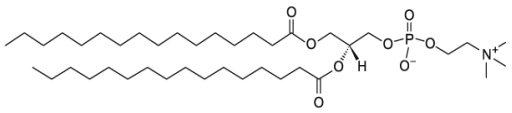	Dipalmitoyl phosphatidylcholine **(DPPC)**
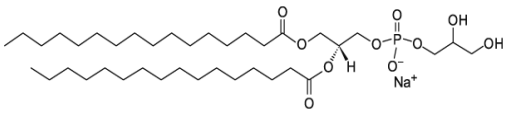	Dipalmitoyl phosphatidyl glycerol **(DPPG)**
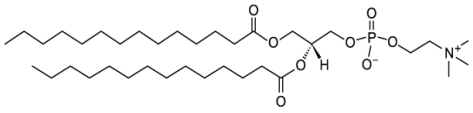	Dimyristoyl phosphatidylcholine **(DMPC)**
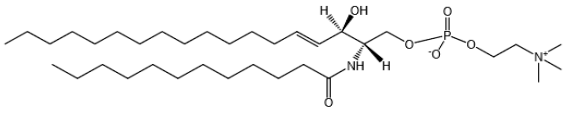	Sphyngomyelin

Table 1. 1: Phospholipids and sphingolipid used in this work

1.2.1 Melting Temperature, T_M

The physical state of the lipids in the membrane can be described by its fluidity. The melting temperature is defined as the temperature required to induce a change in the lipid physical state from the ordered gel phase, where the hydrocarbon chains are fully extended and closely packed, to the less-ordered (also known as the liquid crystalline phase), where the hydrocarbon chains are less organized (BLUME, 1993) (WATSON, 2015).

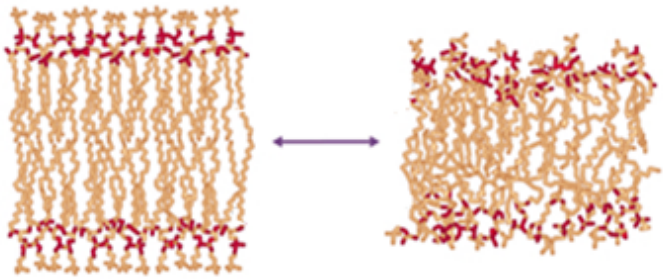

Figure 1.7: A molecular model showing changes in the properties of the lipid bilayer caused by temperature. As the temperature increases, the bilayer passes from a crystalline phase through a gel phase to a liquid crystalline phase. Adapted from (Watson, 2015).

In the gel phase, when the hydrocarbon chains of the phospholipids are stretched out, the chains are extended making it difficult for phospholipids to move laterally. On the other hand, in the fluid phase, when the hydrocarbon chains are bent and their mutual association is weak, phospholipids actively move by molecular motion. (BLUME, 1993; CEVC; MARSH, 1987). Furthermore, at this last case, the membrane permeability, increases, as an indication of a smaller interaction among the phospholipids, induced by temperature.

Examples of displacements (i.e., phospholipid molecular movement) include rotation, lateral and transverse diffusion (flip-flop from one leaflet to the other) of phospholipids. Such active movement of phospholipids rises with temperature and provides the fluidity required to perform various of the biological membranes functions. In addition, the inner and outer leaflets of the natural lipid bilayer are composed by different amount of lipid components, being these differences regulated mainly by lipid flip-flop.(CEVC; MARSH, 1987)

There are several factors which directly affect the melting temperature of lipids, like: hydrocarbon length, presence of saturations, charge and head group species among others. For example, introducing a *cis* double bond into the acyl group establish a kink in the chain, which requires smaller temperature to induce the gel-fluid transition. (CEVC; MARSH, 1987)

The phase transition induces significant changes in lipid membrane structure. In general, the fluid phase, besides being characterized by its higher disorganization, also has a smaller thickness as compared to the gel phase.

Thus, in this study we performed a systematic biophysical study using different experimental techniques in order to infer about the IL interaction of

different vesicles. To do so, we used both zwitterionic as anionic lipids, in order to emulate different cell (and organelles) membranes.

1.3 Goals

1.3.1 General Goal

To investigate the physical influence of 1-14-alkyl-3-methylimidazolium-based IL *[C_{14}MIM][Cl]* in biomimetic membrane systems. To do so, we will perform a systematically experimental study in the absence and presence of the IL, using several experimental techniques.

1.3.2 Specific goals

Characterize the eventual IL toxicity by evaluating some physicochemical properties, like:

- Obtain the structural parameters of the liposomes, by means of Small Angle X-ray Scattering and dynamic light scattering;
- Obtain the melting temperature, T_m, for different lipids in the absence and presence of IL, using fluorescence anisotropy.
- To evaluate the influence of IL on the vesicle surface charge, by means of ζ-potential.

2. Materials and Methods

2.1 Materials

All materials used in this study are listed in Table 2.1 with its reference code and manufacturing batch.

Six different phospholipids and one sphingolipid, the Ionic liquid *[C_{14}MIM][Cl]*, cholesterol and the fluorescent probe DPH (Table 2. 2) are also presented.

	Manufacturer	**Reference code**	**Batch**
POPC	Avanti Polar Lipidis	850457P	160-181PC-193
POPG	Avanti Polar Lipidis.	840457	
DPPC	Avanti Polar Lipidis	850355P	160PC-293
DPPG	Avanti Polar Lipidis	840455	160PG-69
DMPC	Avanti Polar Lipidis	850345	
[C_{14}MIM][Cl]	io-li-tec	IL-0141	J00220.6
DPH	Sigma-Aldrich	1720-32-7	
Cholesterol	Avanti Polar Lipidis	700000P	CH-101
Sphingomyelin	Avanti Polar Lipidis	860062P	BSM-127

Table 2. 1: Materials used in this work.

The ionic liquid 1-tetradecyl-3-methylimidazolium chloride [C_{14}MIM][Cl], was purchased from Io-Li-Tec (98% purity). The 1,6-Diphenyl-1,3,5-hexatrie\ne (DPH, M.W. 232,32) was purchased from Sigma-Aldrich, Inc. (98% purity). The phospholipids 1-palmitoyl-2-oleoyl-sn-glyecro-3-phosphatidylcholine (POPC, M.W. 760.076), 1-palmitoyl-2-oleoyl-sn-glyecro-3-phosphatidylglycerol (POPG, M.W. 770.989), 1,2-dimyristoyl-sn-glyecro-3-phosphatidylcholine (DMPC, M.W. 677.933), 1,2-dipalmitoyl-sn-glyecro-3-phosphatidylcholine (DPPC, M.W.

734.039), 1,2-dipalmitoyl-sn-glyecro-3-phosphatidylglycerol (DPPG, M.W. 744.952), sphingomyelin (M.W. 646.92) and the cholesterol (M.W. 393.70) were obtained from Avanti Polar Lipids, Inc. All lipids were used without any further purification. Special precautions were taken to protect the products for oxidization and hydrolysis, by using only freshly made samples.

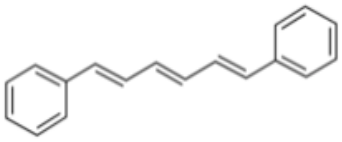	1,6-Diphenyl-1,3,5-hexatriene **(DPH)**
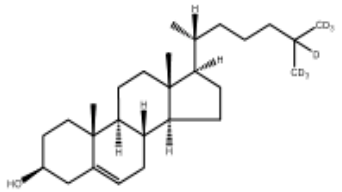	**Cholesterol**

Table 2. 2: Structure of the DPH and cholesterol used in this work.

2.1.1 Sample Preparation Protocols

A stock solution of lipids in chloroform was prepared by dissolving the powder in chloroform (stock lipid concentration ~20 mg/ml). After that, the protocols are different depending on the kind of vesicle that should be prepared (LUVs or GUVs). The stock solutions were freshly prepared to avoid lipid oxidation, in particular for saturated lipids.

Large Unilamellar Vesicles (LUVs):

Aliquots of the stock solution were dried with continuous flow of ultrapure N_2 in test tubes and left for no less than 3 hours in a desiccator under reduced pressure for complete evaporation of the solvent. Next, samples were hydrated with ultrapure water (18.2 MΩ. cm, Milli-Q-Millipore) at temperatures higher than T_M and vigorously vortexed. To induce unilamellar liposomes formulation and

control vesicle's size, all samples were extrused, at least 31 times (also in a temperature higher than T_M), using 50 nm filters with an automated home-made system (Figure 2.1) designed and constructed by the technician Marcelo Everaldo Frade, from the Biosystems Laboratory at the Biophysics Group.

Figure 2.1: Automated system for extrusion. This equipment was developed in our own Lab, designed and constructed by Marcelo Everaldo Frade, from the Biosystems Laboratory at the Biophysics Group.

On the other hand, to prepare the ionic liquid's stocks solution was simpler. All ionic liquids used were added to ultrapure water and vortexed until it was absolutely dissolved. Due to its ionic characteristic, the sample preparation was straightforward.

The ionic liquid was added to the solution after the vesicles were extrused. To be sure about how long the IL takes to interact with vesicles, some tests were performed. This tests are presented in the appendices B.

Giant Unilamellar Vesicles (GUVs): aliquots of lipids in chloroform are placed on glass plates (10 x 3 cm) covered by Indium Tin Oxide (ITO) film, which provides a conductive surface. The conductive sides of ITO are separated by a Teflon spacer of ~2mm thickness containing a small hole that allow inserting a syringe. Plates with the aliquots are subjected to 30 minutes in vacuum to

guarantee the total solvent evaporation. After that, the cell is filled with a 200mM sucrose (Sigma Aldrich, 99% purity) solution.

Alternating voltage generator connected in the blade ends was used to generate an oscillating voltage of ~1V at frequency of 10Hz for 3 hours to stimulate the GUV formation. The apparatus can be appreciated in Figure 2.2. Following, a small volume of the resultant GUV-sucrose solution (~50 μl) is transferred to an Eppendorf containing a 200mM glucose solution. This last step is very important because the density difference between the glucose and the sucrose forces the vesicles to settle at the bottom of the microscopy blade, and the difference in refractive index of both produces a good optical contrast.

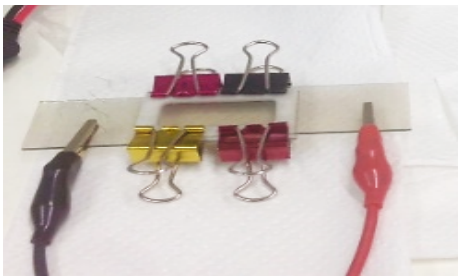

Figure 2.2: Eletroformation Method. Alternating voltage generator connected to the blade ends to generate an electric field.

All this sample preparation was performed at room temperature, thus the GUVs studies were performed with POPC and POPG, both being at fluid phase at room temperature.

2.2 Methods

In this chapter, theoretical features of the experimental techniques employed in this thesis are briefly presented. The approach is intentional to be fully comprehensive and aimed to clarify some of the key concepts used in the data analysis.

2.2.1 The water molecule

In order to understand the behavior of biologically relevant systems, one should understand hydrogen bonding. The ubiquitous and perhaps simplest example of a hydrogen bond is between water molecules. The water molecule is assembled by two hydrogen atoms sharing their electrons with one atom of oxygen, in a specific geometry (Figure 2.3).

The shared electrons are slightly delocalized towards the oxygen atom rather than the hydrogens ones, causing a positive (and negative) charge difference in each hydrogen (or oxygen) atoms (KOTZ; TREICHEL; WEAVER, 2005). (ATKIN; PAULA, 2006). Due to its electric dipole, H_2O has the ability to interact with neighboring molecules by hydrogen bonds (dipole-dipole interaction).

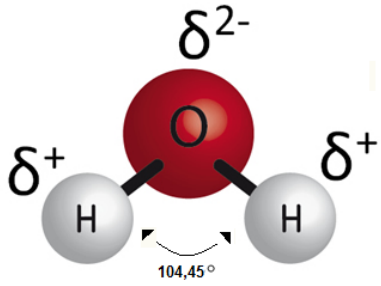

Figure 2.3: Water molecule. Fonte: http://www.breakingifes.com.br/2014/11/funcoes-inorganicas.html

2.2.1.1 Surface Tension

Surface tension is related to the force that must be overcome to transposes a liquid surface. The greater the type of the intermolecular compounds interaction, higher the surface tension (DALTIN, 2011).

There are several surface tension measurement methods through various physical magnitudes such as force, pressure and deformation of the surface. The method used in this study was the Wilhelmy plate.

Wilhelmy Plate Methodology

The Wilhelmy plate, a rectangular plate, is positioned vertically and near to liquid surface (Figure 2.4). The plate's underside is immersed in the liquid and the tensiometer measures the force required to move it vertically upwards as illustrated in Figure 2.4.

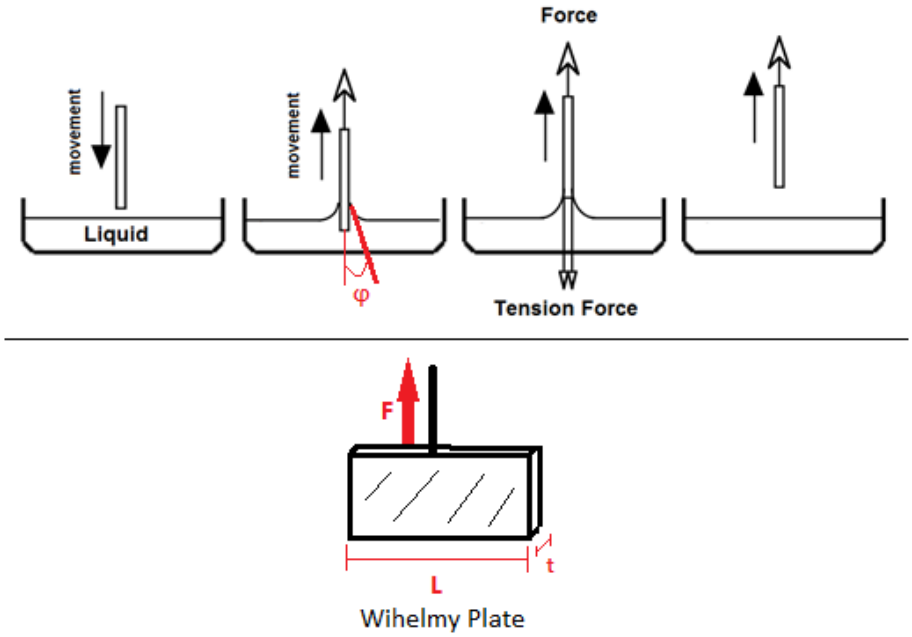

Figure 2.4: Wilhelmy plate method. Adapted from (SALAGER, JEAN L, ANTON, 2005)

Accordingly, the surface tension is proportional to the force exerted to move the plate vertically, and the perimeter of the plate, as well as the contact angle between them and can be written as (CHEN et al., 1998; ISRAELACHVILI, 1991; SAUER; DIPAOLO, 1991; SELL; NEUMANN, 1966)

$$\gamma = \frac{F}{2(L+t).cos\phi} \qquad \textbf{(2. 1)}$$

where F is the force, φ the angle between the plate, and the liquid and 2 (L + t) is the perimeter of the plate in contact with the liquid. Normally the thickness t << L and φ ≈ 0. (BUTT; GRAF; KAPPL, 2003)

Here we were interested in obtain the [C_{14}MIM][Cl] critical micelle concentration (CMC). To do so, we adopted the force tensiometer K100 (KRÜSS FAPESP 2010/51219-4) (Figure 2.5) belonging to the Chemistry Institute of USP under the responsibility of Prof. Dra. Denise Petri. The surface tension was measured by the Wilhelmy plate method.

Figure 2.5: Force Tensiometer K100 - (KRÜSS FAPESP 2010/51219-4)

2.2.2 ζ-Potential

In a solvent, a charged particle will attract ions of opposite charge. The amount of ions decreases with the distance from the reference particle increases. The net charge at the particle surface affects the distribution of ions in the

surrounding region (HUNTER, 1981). Therefore, the liquid layer surrounding the particle exists as an inner region, called the Stern layer where the ions are strongly bound to the particle surface, and an outer region where they are less attached (Figure 2.6) (HUNTER, 1981).

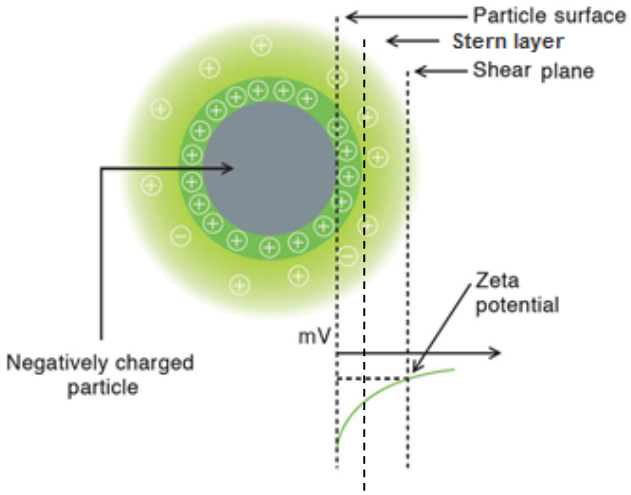

Figure 2.6: Schematic ζ-potential. Adapted from http://laser.spbu.ru/en/research-eng/dzeta-eng.html

When the particle moves, ions within the boundary move with it (i.e. the Stern Layer). This boundary between the Stern layer and the slipping plane defines a region, the electric potential at this point is known as the ζ-potential (HUNTER, 1981). The ζ-potential cannot be measured directly and, therefore, is calculated by the particle electrophoretic mobility.

When an electric field is applied across an electrolyte, charged particles suspended in the electrolyte are attracted towards the electrode of opposite charge. Viscous forces acting on the particles tend to oppose this movement. When equilibrium is reached between these two opposing forces, the particles move with constant velocity (BLEES, 2002; HUNTER, 1981) and the total forces resultant is null.

The particle's velocity depends on the electric field, solvent viscosity and dielectric constant of the medium, and, surely, on the ζ-potential. More pragmatically, the ζ-potential depends not only on the surface of the particle, but also on the suspension itself, in addition to its physical and chemical properties such as pH, ionic strength and temperature (HUNTER, 1981).

Furthermore, another interesting point in a ζ-potential profile of a system is the zero point, where the overall charge of the particle is null. Thus, this point is related to the neutralization of the colloidal system, where positive charges are equal to the negative ones, on the particle surface. The neutral point of the systems studied in this thesis will be highlighted in Chapter 3, where the presence of the cationic IL changes significantly the surface charge of the anionic and zwitterionic systems. Moreover, besides IL presence, such neutralization can be achieved by changing the ionic strength, pH, or in the presence of cationic Ionic Liquids, for instance.

After measuring the electrophoretic mobility, the ζ-potential can be determined by using the Henry's equation, as (HUNTER, 1981).

$$\mu = \frac{2\varepsilon\zeta f(ka)}{3\eta} \qquad \textbf{(2. 2)}$$

where μ is the electrophoretic mobility, ζ is the ζ-potential value, η the viscosity of the fluid, ε the fluid dielectric constant and f(ka) is the Henry's Equation. Two methods are generally used as approximations for the Henry's Equation (BLEES, 2002; HUNTER, 1981).

The Smoluchowski's approximation (*f(ka) ~1*) is straightforward for systems containing more than 1mM of salt and used for folded capillary cell when

with aqueous samples (CLOGSTON; PATRI, 2011; HUNTER, 1981). Yet, for small particles (lower than about 100nm) in low dielectric constant media the better approximation is the Huckel's one (*f(ka) ~1.5*) (HUNTER, 1981). In he present study, due to the lipid and IL concentrations, the Smoluchowski's approximation was used.

ζ- potential experiments were performed with a ZetaSizer Nano-ZS90 (Malvern, FAPESP 09/53074-6) apparatus (Figure 2.7). The device is equipped with a 4mW He-Ne laser with a wavelength of 633 nm and a fixed detector at 90°. The temperature is controlled in the range of 0 to 120 ° C, yet the temperature was fixed at 25°C. For the ζ-potential measurements, a folded capillary cell (DTS1061, Malvern, UK) was used. The total concentration of the lipids was fixed at 1 mM and different molar reasons (0, 1, 5, 10, 20 and 30 mol%) of the IL were added.

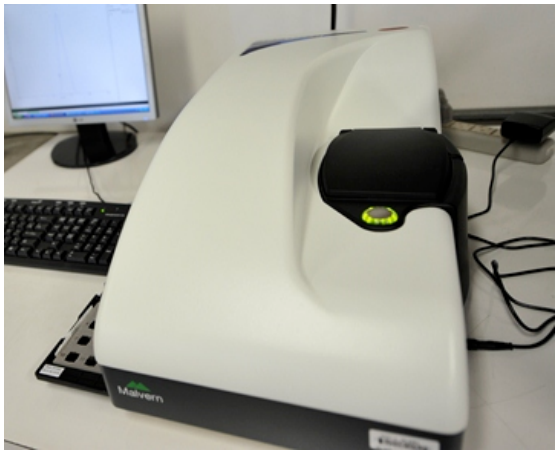

Figure 2.7: ZetaSizer Nano-ZS90 (Malvern, FAPESP 09/53074-6) apparatus

2.2.3 Fluorescence Anisotropy

Some molecules when excited by a polarized electric field can emit photons with a specific polarization. The emission polarization is described by the fluorescence anisotropy (*r*). Hence, fluorescence anisotropy is the phenomenon where the light emitted by a fluorophore has unequal intensities along different axes of polarization. Early pioneers in the field include Aleksander Jablonski, Gregorio Weber and Andreas Albrecht. (LAKOWICZ, 2006)

The origin of such phenomenon is due to the principle of photoselective excitation of fluorophores, i.e., the existence of electrons absorption and emission dipolar moments in specific directions regarding the fluorophore molecule. In an isotropic solution, fluorophores are all randomly oriented. When exposed to polarized light, those molecules that have transition moments components oriented at similar direction as the incident light will be excited. Indeed the probability of excitation will be proportional to cos (θ) (LAKOWICZ, 2006). This implies that the excited state of these electrons are not randomly oriented after the excitation. (LAKOWICZ, 2006).

The depolarization of light can be caused by several phenomena. The most common cause is rotational diffusion around the molecule center of mass. Thus, the fluorescence anisotropy measurements reveals the average angular displacement that occurs between the absorption and the consequent emission of a photon (LAKOWICZ, 2006). Such rotational movements are depended on the system inserted and the surroundings viscosity.

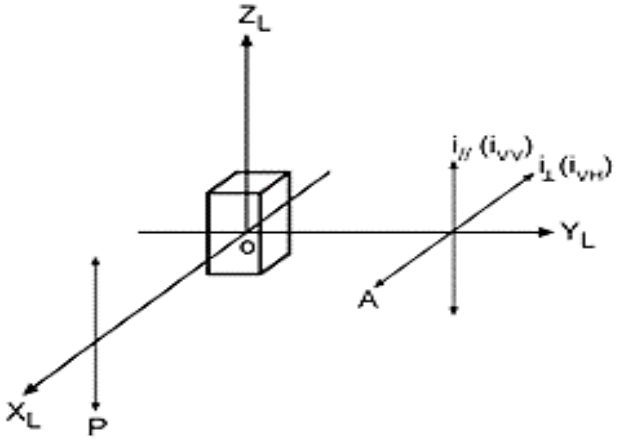

Figure 2.8: The sample placed at the origin of the laboratory reference O is excited through a polarizer P with the principal axis oriented along the ZL axis. The fluorescence emission is monitored through an analyzer A. The analyzer can be rotated so that the principal axis of the analyzer is either along the ZL axis or the XL axis. Adapted from (AMELOOT et al., 2013)

The sample is excited with vertically polarized light parallel to the direction of the z-axis. In the optical path of light emission, polarizers are oriented vertically or parallel to the direction of the polarized excitation. The emission intensity that passes through the parallel oriented polarizer is represented by $I_{\parallel}$ and the one that passes through the perpendicularly oriented polarizer is represented by $I_{\perp}$. By these values, both fluorescence anisotropy (*r*) as well as the polarization (P) can be defined as:

$$r = \frac{I_{\parallel} - I_{\perp}}{I_{\parallel} + 2I_{\perp}} \qquad \textbf{(2. 3)}$$

$$P = \frac{I_{\parallel} - I_{\perp}}{I_{\parallel} + I_{\perp}} \qquad \textbf{(2. 4)}$$

Fluorescence anisotropy and polarization are both expressions for the same physical phenomenon. (LAKOWICZ, 2006).

Nonetheless, for the fundamental anisotropy of one fluorophore, the expression above (eq. 2.3) should be modified. First, consider a fluorophore

without rotational diffusion and that both absorption and emission dipolar moments are parallel, assuming that the angle between these dipolar moments and the z and y axes (Figure 2.9) are θ and ϕ, respectively, it is possible to schematize the problem as follows:

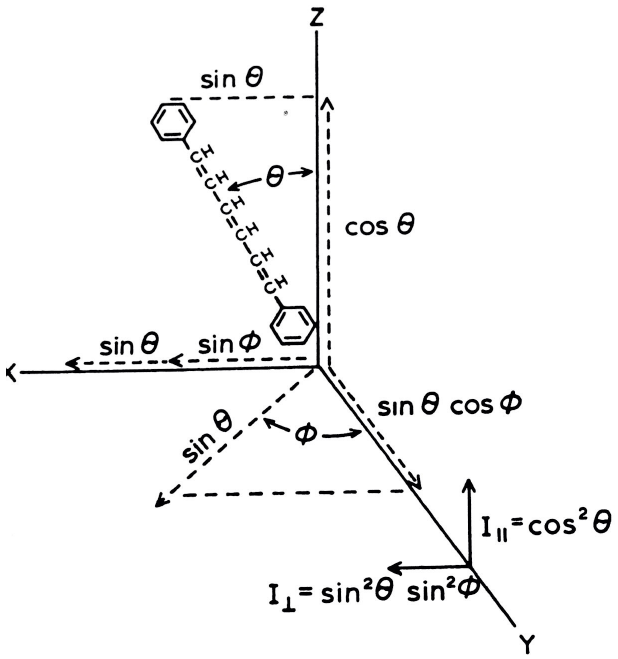

Figure 2.9: V corresponds to the polarizers oriented vertically and H horizontally. VV and HH correspond to parallel-polarized excitation and emission, while VH and HV correspond to perpendicularly polarized excitation and emission. Extracted from (LAKOWICZ, 2006)

In this case, because the emission intensity of a dipole is proportional to its vector projected in the axis of observation and knowing the intensity that passes through a polarizer is proportional to the square of this projection on such axis, it is also possible to write

$$I_{\parallel}(\theta,\varphi) = \cos^2\theta \text{ and } I_{\parallel}(\theta,\varphi) = \sin^2\theta\,\sin^2\varphi \quad \textbf{(2. 5)}$$

Nevertheless, the anisotropy of solutions contains many fluorophores with random distribution is calculated by an average based on the photoselection

principle (already mentioned) and on the contribution of each fluorophore. The dependence of ϕ is eliminated since the population of excited fluorophores will be symmetrically distributed along the z-axis. Then, we can express the fluorescence anisotropy as

$$r = \frac{3 < \cos^2 \theta > -1}{2} \quad \textbf{(2. 6)}$$

The excited population of fluorophores will not be perfectly state and rarely the absorption and emission moments are parallel. Due to that, we must consider an angle (β) between these transition moments and that $< \cos^2 \theta >$ depends on the photoselective excitation of the fluorophores. Thus, the fundamental anisotropy can be written as:

$$r_0 = \frac{2}{5}\left(\frac{3\cos^2 \beta - 1}{2}\right) \quad \textbf{(2. 7)}$$

Observing the fundamental anisotropy value (eq. 2.7) the maximum value of r_0 is 0.4 (if β = 0 °). Moreover, such value should be observed in the absence of other depolarization processes, such as rotational diffusion or energy transfer. Moreover, the fundamental anisotropy is zero when β = 54.7°, i.e., above this value, r_0 become negative and the maximum value for negative anisotropy (-0.20) is found for β = 90 ° (D M JAMESON, 1998).

As already mentioned in the text, several physical phenomena can decrease the fluorescence anisotropy (LAKOWICZ, 2006). The most common cause is the rotational diffusion that occurs during the lifetime of the excited state. Measurements of this parameter give information about the relative angular change of the fluorophore dipolar moments. The effects of rotational diffusion can be decreased if the fluorophore is immersed in the membrane. (LAKOWICZ,

2006). In the present study, DPH was chosen as fluorescent probe for anisotropy measurements (Table 2.2), because of its wide use for purpose for membranes studies (LAKOWICZ, 2006). Its affinity with hydrophobic media and the low solubility in water allows interaction with the phospholipid inner region, both in the gel phase and in the fluid phase. (LAKOWICZ, 2006). Moreover, this molecule has almost parallels absorption and emission dipolar moments, favoring the data interpretation, since for this case $\beta \sim 0^{o}$.

The fluorescence anisotropy measurements were performed using the static fluorimeter Cary Eclipse (Figure 2.10) (Varian FAPESP 01/11721-3) from the Biophysics Group. The apparatus includes a Xenon lamp of 450W as a light source and a detection system comprising a photomultiplier capable of detecting emissions in the range of 200 to 800 nm. Temperature control (water system based) from 0° C to 100° C, enabling to sweep a big range of temperatures and expect to see the decay of anisotropy values as the temperature increases. Samples were conditioned in quartz cuvvetes with 10mmx2mm optical path and choosing the absorption optical path equal to 1mm and emission optical path equal to 5mm in order to avoid multiple scattering.

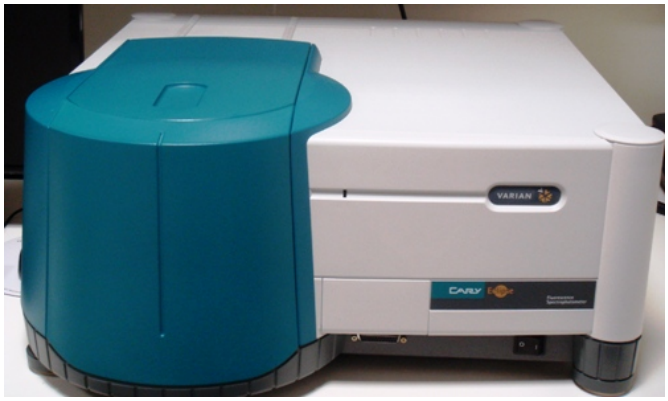

Figure 2.10: Static Fluorimeter Cary Eclipse (Figure 3.3) (Varian FAPESP 01/11721-3).

DPH was solubilized in tetrahydrofuran and conserved in refrigeration. The lipids solution was prepared the same way described earlier in the text. After the lipids were hydrated and extrused, DPH was added and finally the IL. The lipids concentration was fixed at 0,5mM and the final volume of added tetrahydrofuran was always < 0.2% v/v. For these measurements, the excitation and emission wavelengths were set to λ_{exc} = 365nm and λ_{emi} = 430nm, respectively, whereas both excitation and emission slits were set to 2.5nm.

2.2.4 Dynamic light scattering (DLS)

Dynamic light scattering (DLS) is usually applied for the structural characterization of particles, emulsions and larger molecules dispersed or dissolved in a liquid. This technique measures the translational diffusion coefficient due to the particles Brownian motion and relates it to particles size (PECORA, 1993).

DLS technique analyses the intensity fluctuations of the scattered light at a fixed angle (generally 90^{o}, but there are other configurations). The relationship between the scattering particle size (hydrodynamics radius) and the diffusion coefficient is defined by the Stokes-Einstein equation (PECORA, 1993). Surely it's a rough approximation and it takes into account that the particles are spheres and only the Brownian motion is responsible for particle movement. Under such assumptions it is possible to write (PECORA, 1993):

$$D = \frac{k_B T}{6\pi\eta r} \qquad \textbf{(2. 8)}$$

where T is the absolute temperature in Kelvins, η the sample's viscosity and k_B the Boltzmann's constant (~ $1.38x10^{-23}$ $J.K^{-1}$). The particle size got from this technique is the hydrodynamic radius.

The Polydispersity index (PDI) gives a rough estimation on the particle sizes distribution. This dimensionless index is related to the dispersity of the sample in such a way that values smaller than 0.05 are rarely seen other than with highly monodisperse standards. Also, values greater than 0.5-0.7 indicate that the sample has a very broad size distribution and is probably not suitable for the DLS measurements.

In this study, DLS experiments were performed on the ZetaSizer Nano-ZS90 (Malvern, FAPESP 09/53074-6) apparatus (Figure 2.7), with fixed temperature at 25°C and the acrylic cuvette of 10mmx10mm.

2.2.5 Small Angles X-ray scattering (SAXS)

Small Angle X-ray Scattering (SAXS) is a well-established method of studying structural characteristics, such as shape, size and possible interactions among particles. (CHU; HSIAO, 2001; RUBIM, 2014; SCHNABLEGGER; SINGH, 2013).

Conceptually, SAXS experiment is rather simple: X-rays illuminate a sample and a detector registers the scattered radiation. A simplified experimental set-up is shown on Figure 2.11.

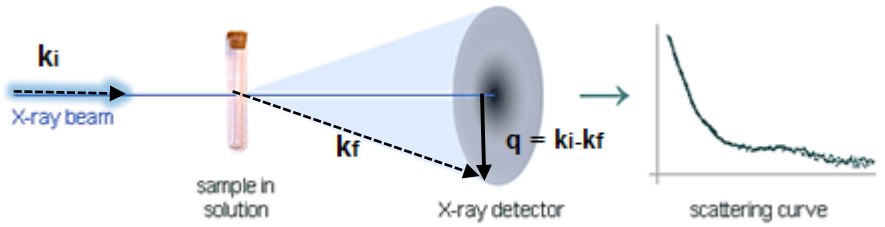

Figure 2.11: Scheme of sample illuminated by X-rays and the scattered radiation registered by a detector. Usually a "beam stopper" is used to protect the detector, which prevents non-interacting radiation from damaging the sensor due to its high intensity. Extracted from http://biosaxs.com/technique.html

A monochromatic beam with incident wave vector $\overrightarrow{k_i}$ interacts with the sample (Figure 2.11). The scattered intensity is collected as a function of the so-called scattering angle 2θ. Zero energy transfers characterize elastic interactions, such that the final wave vector $\overrightarrow{k_f}$ is equal in modulus to incident wave vector $\overrightarrow{k_i}$. The relevant parameter to analyses the interaction is the momentum transfer or scattering vector $\vec{q}$, where $\vec{q}$ is defined as the difference between the incident and the scattered wave vector (FEIGIN; SVERGUN, 1989) and can be written as:

$$q = \overrightarrow{k_i} - \overrightarrow{k_f} = \frac{4\pi \sin\theta}{\lambda} \qquad \textbf{(2. 9)}$$

ranged from q_{min} = 0.02 Å^{-1} to q_{max} = 0.33 Å^{-1}.

Since the studied systems are not crystalline, the interpretation of the scattering intensity requires greater care. The scattered intensity can be theoretically modelled as the multiplication of both P(q) and S(q), as

$$I(q) = N < P(q) >< S(q) > \qquad \textbf{(2. 10)}$$

where N corresponds to the number of scattering centers, P(q) is the form factor, which contains information about the scattering particle size and shape, whereas S(q) is the structure factor that relates the interaction between adjacent particles.

For cases in which there is no correlations among the scattering centers or those correlations could be neglected, S(q) ≈ 1 (EISBERG; RESNICK; BROWN, 1986; FEIGIN; SVERGUN, 1989).

The experimental scattering intensity is usually fitted by a theoretical model, in order to (at least generally) determine the scattering particle electronic density profile ρ(r), which in turns will be related to the scattering particle size, shape (maximum dimension), as well as any eventual interactions among the scattering particles (FEIGIN; SVERGUN, 1989). The software we used to analyze the SAXS curves was GENFIT, developed by Prof. Francesco Spinozzi, from *Università Politecnica delle Marche* (SPINOZZI et al., 2014). The software fits several experimental curves, concomitantly, by the selection of one or more theoretical models (SPINOZZI et al., 2014).

In order to fit our scattering curves, we used the well-known three-step-model for an infinite plan to describe the electron density profile and, as a consequence, the scattering curves. One should bear in mind that the vesicle radius is much larger than the X-ray wavelength and under this assumption it is possible to assume that the vesicle is, in fact, an infinite flat structure (DOMINGUES et al., 2013). Following such procedure, it is possible to write the total scattering intensity as:

$$I(q) = k\frac{A}{q^2}\,P_t(q) \qquad \textbf{(2. 11)}$$

where *k* and *A* are constants related to lipid concentration and on the experimental setup, respectively. $P_t(q)$ is the so-called cross-section form factor and can be analytically obtained in the three-step model.

Such theoretical model considers that LUVs do not have a homogenous electronic density profile along the z-axis of the bilayer. It splits each leaflet of the bilayer into three different regions regarding the electron density profile. The most inner region of the leaflet is called CH_3, followed by the CH_2 and polar regions (Figure 2.12 e Figure 2.13) (DOMINGUES et al., 2013; FERNANDEZ et al., 2008). Each of them has its own electron density value (ρ_i, being *i* a representation of CH_3, CH_2 or polar regions) as well as its own thickness (R_i).

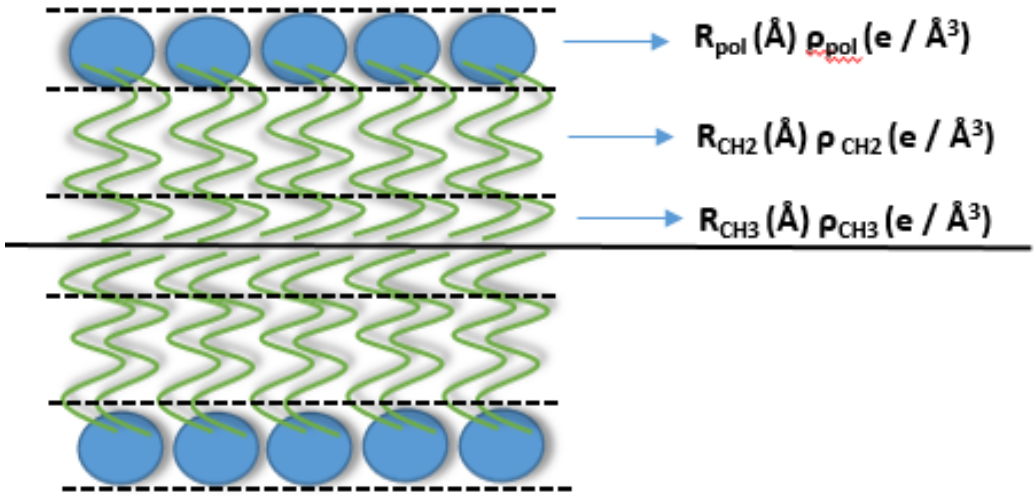

Figure 2.12: SAXS adjustment parameters along the z-axis of the bilayer. The most inner region of the leaflet is CH_3 region, followed by the CH_2 and polar region.

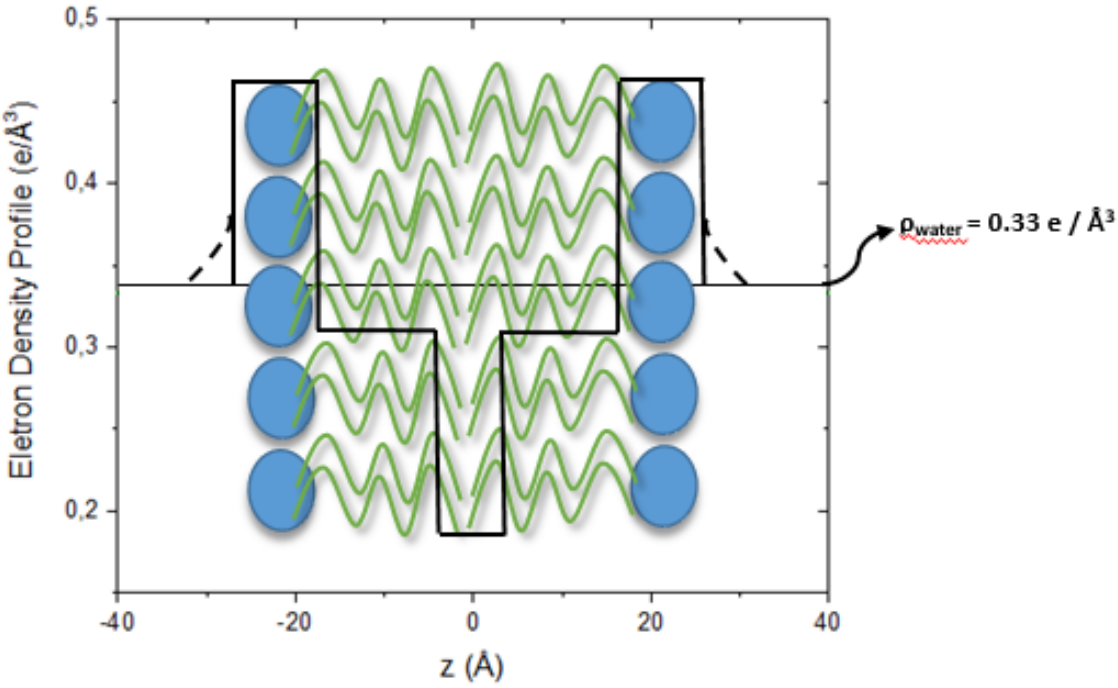

Figure 2.13: Electronic density profile along the z-axis of the bilayer. It splits each leaflet of the bilayer into three different regions regarding the electron density profile. The most inner region of the leaflet is called CH_3, followed by the CH_2 and polar region.

Thus, in order to reproduce the experimental scattering curve, we need to adjust these six parameters (ρ_i and R_i, for each region) for each scattering curve. By doing so the cross section form factor can be written as:

$$P_t(q) = \left\{ \frac{2}{q} \{ \Delta\rho_{CH_3} \sin R_{CH_3} + \Delta\rho_{par} [\sin q \left(R_{par} + R_{CH_3}\right) - \sin q\, R_{CH_3}] + \Delta\rho_{pol} [\sin q \left(R_{pol} + R_{par} + R_{CH_3}\right) - \sin q \left(R_{par} + R_{CH_3}\right)] \} \right\}^2 \quad \textbf{(2. 12)}$$

where $\Delta\rho_{CH3} = \rho_{CH3} - \rho_{water}$, $\Delta\rho_{par} = \rho_{par} - \rho_{water}$ and $\Delta\rho_{pol} = \rho_{pol} - \rho_{water}$ ρ_{wate} the water, ρ_{par} acyl chain and polar head electronic density respectively (Figure 2.13) (DOMINGUES et al., 2013).

In order to avoid over interpretation of SAXS data, some of these fitting parameters were allowed to vary within a narrow range: R_{CH3} (2.0 Å < R_{CH3} < 3.5 Å), ρ_{CH3} (0.15 e/Å^3 < ρ_{CH3} < 0.25 e/Å^3) and ρ_{par} (0.25 e/Å^3 < ρ_{par} < 0.30 e/Å^3), in accordance with data from the literature (DOMINGUES et al., 2013; FERNANDEZ et al., 2008). The electron density of water was fixed (=0.334e/ Å^3) along the fitting process. As mentioned earlier in the text, all SAXS fitting were performed by using GENFIT (SPINOZZI et al., 2014).

SAXS measurements were carried out in this work were performed at the National Laboratory of Synchrotron Light (LNLS), Campinas, SP, Brazil specifically in the SAXS-1 (D11A) beamline. The sample-to-detector distance was ~1000mm and the temperature 22±1°C. The experimental scattering curves were corrected for water contribution as well as sample's attenuation. The total lipid concentration was fixed at 10mM in the absence and presence (0, 15, 30 and 45 mol%) of the IL.

2.2.6 Optical Microscopy

In order to visualize the GUVS, an optical inverted microscope Axiovert 200 (Zeiss FAPESP 2015/50680-5) under the responsibility of Prof^a Rosangela Itri from the Laboratório de Cristalografia at the Physics Institute (USP) was used (Figure 2.14).

Figure 2.14: Optical inverted microscope Axiovert 200 (Zeiss FAPESP 2015/50680-5).

This microscope uses a halogen lamp and a set of lenses to allow GUVs visualization. It has three different lenses (10x, 40x and 63x) and several inner filters that can be used for fluorescence microscopy. Nevertheless, in the present study only the phase contrast mode was used and all images presented in this study were recorded with a *Zeiss AxioCam MRm camera*. Figure 2.15 shows an example of image from the microscope used.

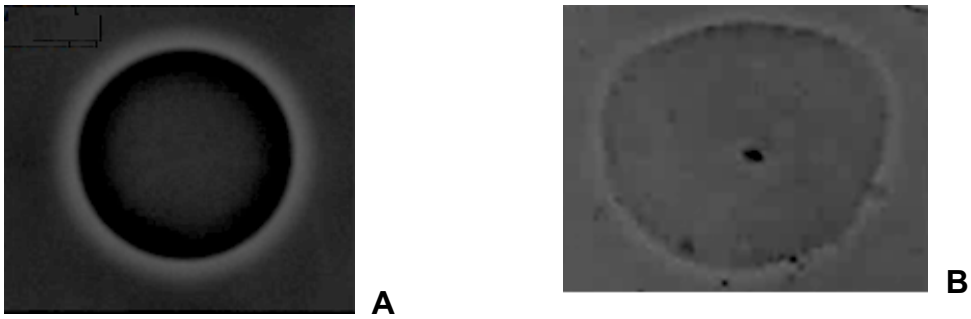

Figure 2.15: Phase contrast mode. (A) due to the differences between the inner and out sugar solution the contrast is higher compared to (B) that for some reason the inner and outer sugar solutions mixed up and the contrast is lost

GUVs are visualized in the microscope in the presence of two different sugar solutions, being one inside the vesicle and the other outside of the GUV,

namely respectively, sucrose and glucose. Moreover, in order to guarantee the vesicle integrity, both sugar solution must be isotonic, to avoid vesicle deformation or eves disruption due to osmosis.

In the phase contrast mode, the biomimetic membrane can be easily visualized, due to the differences between the inner and out sugar solution, as evidenced in Figure 2.15 A. On the other hand, if by some reason the inner and outer sugar solutions mixed up, due to the presence of pores on the vesicle surface or vesicle rearrangement for example, such contrast is lost (Figure 2.15 B).

3. Results and Discussion

3.1 Surface Tension of [C_{14}MIM][Cl]

First, in order to better understand the behavior of [C_{14}MIM][Cl] in solution, surface tension measurements were performed in collaboration with prof. Denise Petri and the Ph.D. and the student Juliana Raw. As mentioned earlier in the text, the increase of amphiphilic molecules in the air/water interface increases the probability of micelle formation and decreases the solution surface tension. Such behavior is related to the CMC.

The superficial tension measurements for the water and the buffer sodium acetate-phosphate-borate, 20 mM, pH 7.0, was measured at several IL concentrations. The temperature was fixed at 25^{o}C and the concentration of the IL [C_{14}MIM][Cl] was increased from 0mM to 9.62mM

The measurements were performed in the absence and presence of buffer solution, to avoid pH variation during IL incorporation. CMCs values were obtained through the experiment of surface tension by varying the concentration of ionic liquid (by titration) in water and in buffer at 24.0±0.1°C. The results are showed in Figure 3.1.

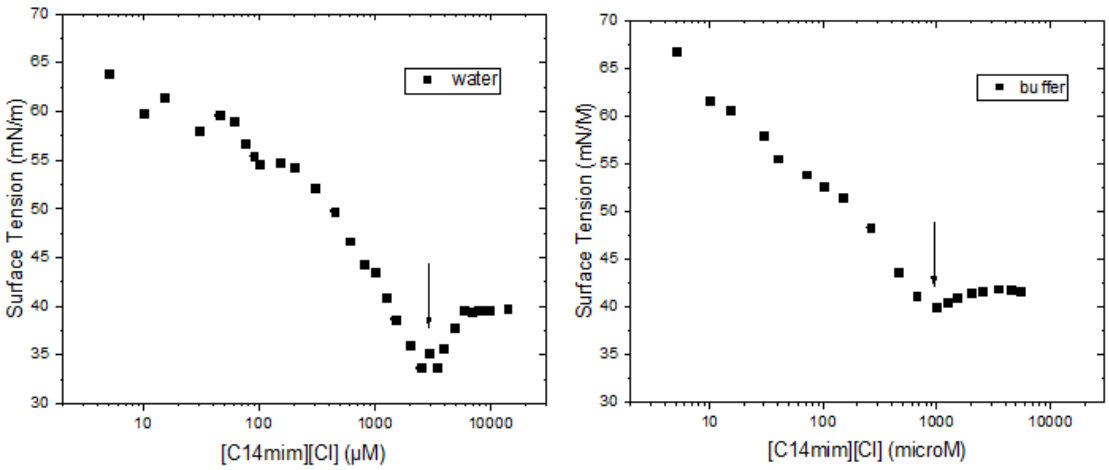

Figure 3.1: Mean surface tension of [C_{14}MIM][Cl] in water (left) and in buffer (AC, FO, BO pH 7.25) (right)

Figure 3.1 shows the decrease of the surface tension as [C_{14}MIM][Cl] concentration increases. There is a quite evident minimum value around 3000 μM and 1000 μM for water and buffer systems, respectively. The minimums indicated by the black arrow is due to impurities present in the IL solution, which is only 98% pure.

This result is expected since the IL is an amphiphilic molecule that has a surfactant like behavior. The CMC obtained in water is equal to 3.0 ± 0.1 mM and is consistent with the value reported in the literature (ŁUCZAK et al., 2008; MISKOLCZY et al., 2004). Otherwise, in the presence of buffer this value is smaller than expected, and equal to 1.0 ± 0.1 mM. The smaller value is also coherent since the addition of salt to the system (buffer) reduces the electrostatic repulsion among surfactant molecules, favoring the micelle formation.

3.2 ζ-Potential

ζ-potential measurements was obtained as key indicator of superficial charge of the liposomes and, as a consequence, the stability of the colloidal

dispersion . For high values of ζ-potential (|ζ|> 30mV), the particles repels each other causing particle stability. The lower, closer the particles can get and more unstable the system is considered (CLOGSTON; PATRI, 2011; MARSALEK, 2012; NANOCOMPOSIX, 2012). Since [C_{14}MIM][Cl] has a positive charge, because of the presence of imidazolium on the hydrophilic head, the IL would interact majorly with the vesicles with negative surface charge. Here, we made sure to use concentrations of IL under the CMC (critical micellar concentration) to assure the [C_{14}MIM][Cl] would not form micelles in solution.

3.2.1 Anionic Vesicles

To make sure the effect of the IL is independent of lipids concentration, we tested two different concentrations for DPPC and a mixture of DPPC:DPPG at 1 mM and 2 mM. In Figure 3.2, these two systems are shown. The ζ-potential values were similar regardless the lipids concentration. Therefore, the lipid concentration does not alter significantly the IL effect for these two systems.

For the all negative charged vesicles, the influence of [C_{14}MIM][Cl] is evident. For DPPG, the ζ-potential increased from -61.5mV without IL to 66.9mV in the presence of 30mol% of IL for 1mM. The DPPG neutral point (described in 2.2.2) is 8.13mol% for 1mM and 11.17mol% for 2 mM. So is necessary ~0.082 mM of IL, to neutralize 1mM vesicle and ~0.112 mM to neutralize 2mM vesicle of DPPG.

Consistently, the mixture of DPPC:DPPG needed approximately half of the concentration of [C_{14}MIM][Cl] (3.5mol%, equivalent to 0.035mM) to be neutralized, which match nearly with the proportion of negative charge. For the

mixture, the ζ-potential value changed from -71.3±0.1mV to 67.3±0.1mV in the presence of 30mol% of [C_{14}MIM][Cl] for 1mM.

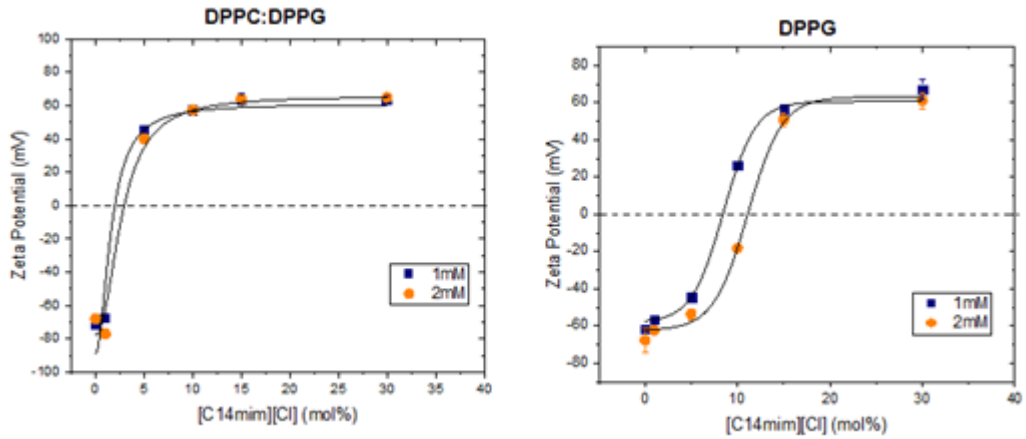

Figure 3.2: ζ-potential by the increase of [C_{14}MIM][Cl] concentration for 1mM and 2mM of DPPG (left) and DPPC:DPPG, at molar reason 1:1 (right).

Figure 3.3 shows the electrophoretic analysis, presented by the ζ-potential values versus the variation of [C_{14}MIM][Cl] concentrations (0,1,5,10,15,30 mol%), for both POPG and POPC:POPG. Here one can notice a jump between the zeta potential values of 0mol% and 1mol%. Probably this behave is due to the charge shielding that occurs as the IL is added.

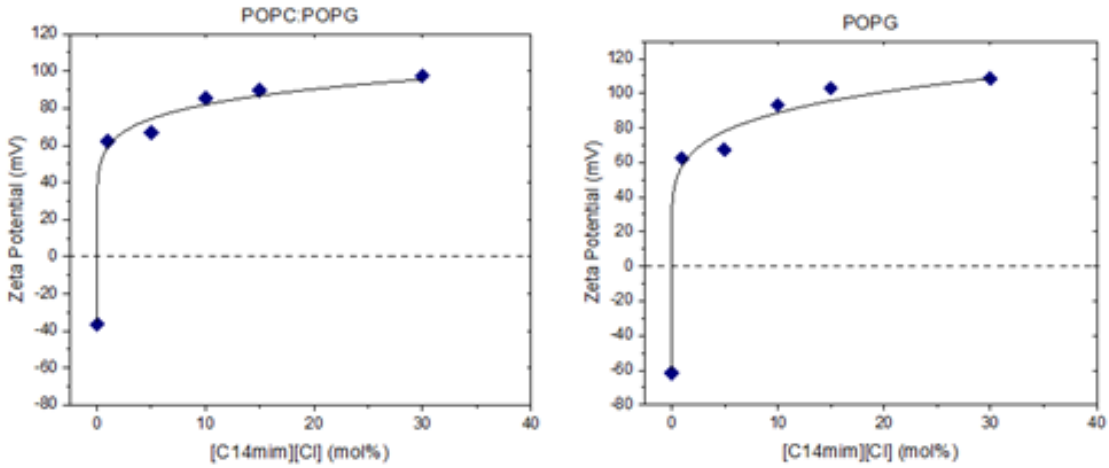

Figure 3.3: ζ-Potential versus [C_{14}MIM[]Cl] concentration of POPC:POPG (left) and POPG (right) at molar reason 1:1

For POPG and POPC:POPG the effect was smaller than compared to DPPG and DPPC:DPPG vesicles. For POPG the ζ-potential increased from -61.9±0.1mV in the absence of IL to 109.6±0.1mV in the presence of 30mol% of IL (for [POPG]=1mM), and the neutral point was ~0.04mol%. This can be explained by the abrupt increase of the ζ-potential between 0mol% and 1mol% Thereby, the mixture of POPC:POPG needed 0.22mol%, to be neutralized, also related to the sudden boost between 0mol% and 1mol%. For the mixture, the ζ-potential value changed from --37.9±0.1mV to 97.7±0.1mV in the presence of 30mol% of [C_{14}MIM][Cl].

3.2.2 Zwitterionic Vesicles

The same concentration test applied to DPPG and DPPC:DPPG liposomes was employed to DPPC also at 1mM and 2mM (Figure 3.4). In this case the ζ-potential values at 1mM and 2mM where different after 1mol%, but the difference was not significant and, therefore, we considered the concentration of the lipids do not alter the effect of the IL. Here one can also notice a jump between the zeta potential values of 0mol% and 1mol%. Probably this behave is due to the charge shielding that occurs as the IL is added.

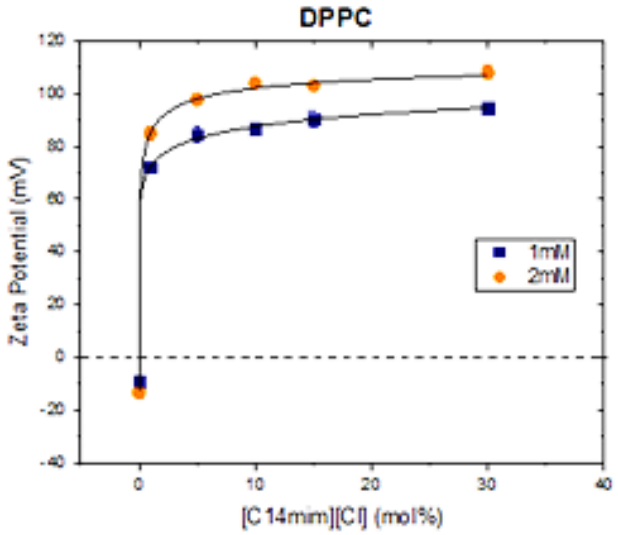

Figure 3.4: ζ-potential of DPPC at 1 mM (black squares) and 2mM (red circles).

For zwitterionic vesicles composed by DPPC, the ζ-potential value in the absence of IL at 1mM is -9.1±0.1mV and at 2mM is -13.5±0.1mV. The addition of [C_{14}MIM][Cl] contributes to increase of the ζ-potential value (Figure 3.5). For DPPC with 30 mol% (0.3mM) of IL, the value enhance to 94.7±0.1mV at 1mM and to 108.0±0.1mV at 2mM, showing the presence of the IL alter the ζ-potential values to more positive ones.

The mixture of DPPC:DMPC as well as DMPC were also measured. Results can be seen in Figure 3.5.

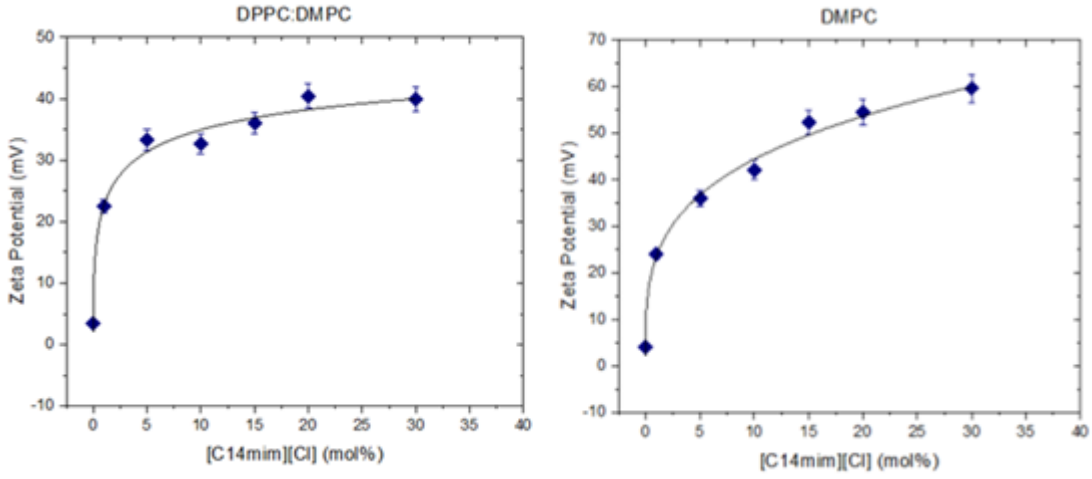

Figure 3.5: ζ-Potential versus [C_{14}MIM[]Cl] concentration of DPPC:DMPC (left) and DMPC (right) at molar reason 1:1

After a certain concentration amount of IL, a significant tendency of saturation can be noticed, and after 1 mol% the ζ-potential value tends to reach a plateau. The same occurs to POPC (Figure 3.6). Systems composed by POPC:SM:Ch were evaluated in the presence of [C_{14}MIM][Cl].

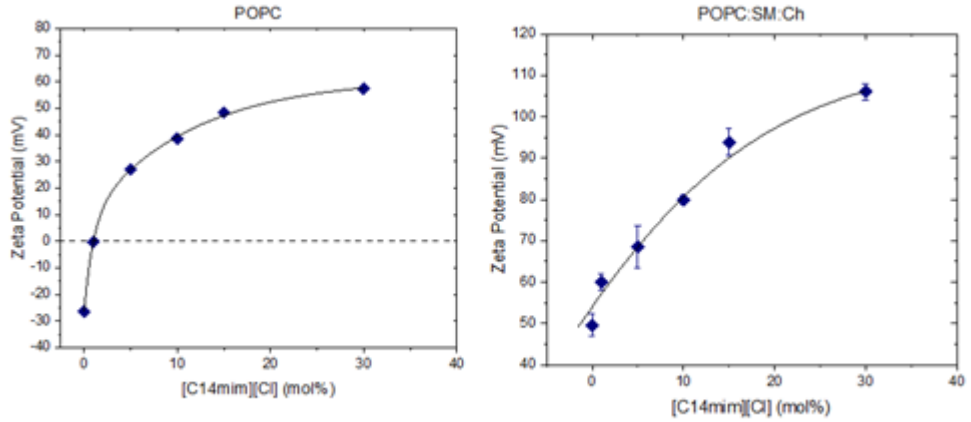

Figure 3.6: ζ-Potential versus [C_{14}MIM[]Cl] concentration of POPC (left) and POPC:SM:Ch (right) at molar reason 1:1:1.

Similarly to DPPG and POPG, POPC vesicles in the presence and absence of cholesterol (and sphingomyelin) did not shown interaction as strong as the DPPC (Table 3. 1). However, the presence of IL increases the positive charge at the surface of the liposomes. With these results is clear the IL changes the superficial charge of the liposome increasing the ζ-potential value and, as consequence, change its instability. As can be seen in Table 3. 1, for anionic vesicles, the variation of ζ-potential value is higher than compared to zwitterionic vesicles.

System	$\Delta\zeta = \zeta - \zeta_0$ (mV)
DPPG	128.4±0.1
DPPC:DPPG	138.6±0.1

POPG	171.5±0.1
POPC:POPG	135.6±0.1
DPPC	103.8±0.1
DPPC:DMPC	35.9±0.1
DMPC	55±0.1
POPC	81±0.1
POPC:SM:Ch	57±0.1

Table 3. 1: ζ-potential variation by 30 mol% of IL.

3.3 Fluorescence Anisotropy

The fluorescence probe DPH is known to penetrate the hydrophobic core of the lipid bilayer (ANDRICH; VANDERKOOI, 1976). This means that when DPH is inserted into the bilayer it can absorbs polarized photons and re-emits also s polarized light, which in turn reflects its molecular movement inside the membrane. Thus, the thermodynamic behavior (or T_M value) of the bilayer was studied in the presence of $[C_{14}MIM][Cl]$. Here, we made sure to use concentrations of IL under the CMC (critical micellar concentration) to assure the $[C_{14}MIM][Cl]$ would not form micelles in solution.

In order to use the better ratio of probe:lipids that would favor the interaction between them, DPPC and DPH were tested at three different molar ratios: 1: 25, 1: 50 and 1: 100. From all studied concentrations, there was no significant change in the DPPC thermodynamic behavior in a function of DPH concentration, and the curves were similar (Figure 3.7).

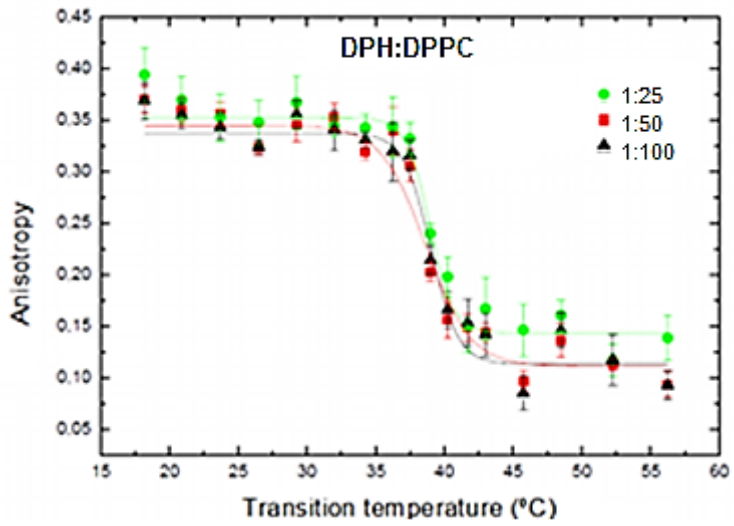

Figure 3.7: Anisotropy of different proportions of DPH: DPPC

The molar ratio of 1:50 was chosen to the follow experiments in order to avoid both low intensity (caused from insufficient probes as in the case 1: 100) and saturation (caused by high amount of probe as in case 1 : 25).

Since the melting temperature of POPC and POPG is around -2°C, it was not possible to study these two lipids using fluorescence anisotropy. For that reason, we measured the anisotropy of DPPC, DMPC and DPPG to obtain T_M. First the fluorescence anisotropy of the zwitterionic vesicles were measured in the absence and presence of 0, 10, 20 and 30mol% of [C_{14}MIM][Cl]. However, for the negative charged vesicles, the anisotropy had a big variation between 0mol% and 10mol%. Hence, for these liposomes, we explored this interval (2, 4, 6 and 8mol%).

3.3.1 Zwitterionic Vesicles

Figure 3.8 shows the anisotropy values versus the temperature in Celsius degree. As the concentration of [C_{14}MIM][Cl] increases, there is no great variation in the melting temperature, and in the case of DPPC:DMPC, the curves overlap.

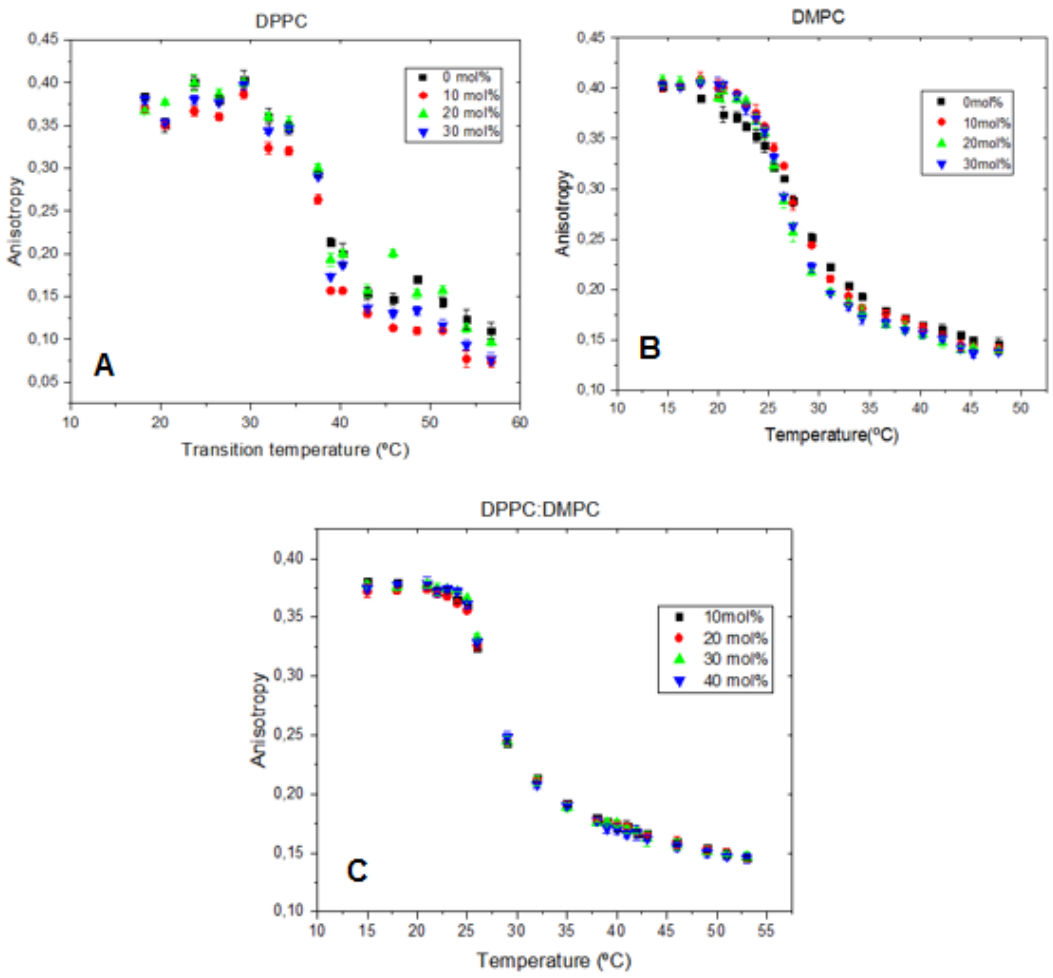

Figure 3.8: Anisotropy versus temperature (ºC) as [C_{14}MIM][Cl] is add to DPPC, DMPC and DPPC:DMPC at 0.5mM.

Concerning the system composed by DPPC, the difference between no IL and 30mol% of IL was ~0.9ºC (Figure 3.8 A), whereas for DMPC was ~1.3 ºC (Figure 3.8 B), both small. For DPPC:DMPC the T_M change was ~0.6ºC (Figure 3.8 C). Therefore, no significant change in T_M was observed, and the values were similar at all concentrations. The mean melting temperature was 38ºC for DPPC and approximately 27.75ºC for DMPC.

To better visualize the T_M variation, Figure 3.9 exhibit the melting temperature as function of IL concentration. The lines are purely eye guides and have no physical meaning.

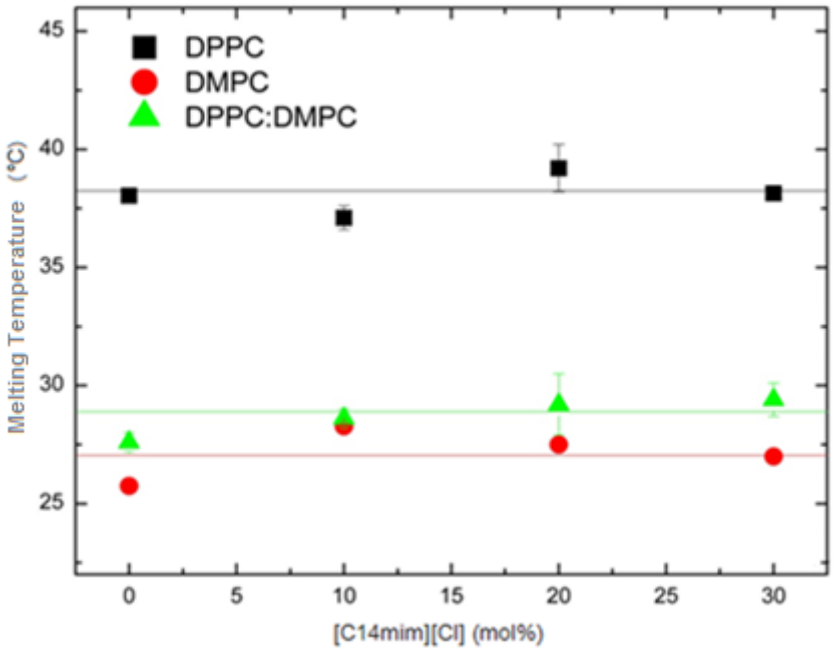

Figure 3.9: Melting temperature variation as function of [C_{14}MIM][Cl] concentration for DPPC, DMPC and DPPC:DMPC. The lines are purely to guide the eyes and have no physical meaning.

3.3.1 Anionic Vesicles

In contrast to the zwitterionic vesicles, negatively charged vesicles have a significant change in the melting temperature value. By Figure 3.10, is clear the melting temperature decays for DPPG and DPPC:DPPG as IL concentration increases. The lines has no physical meaning and are purely to eye guides.

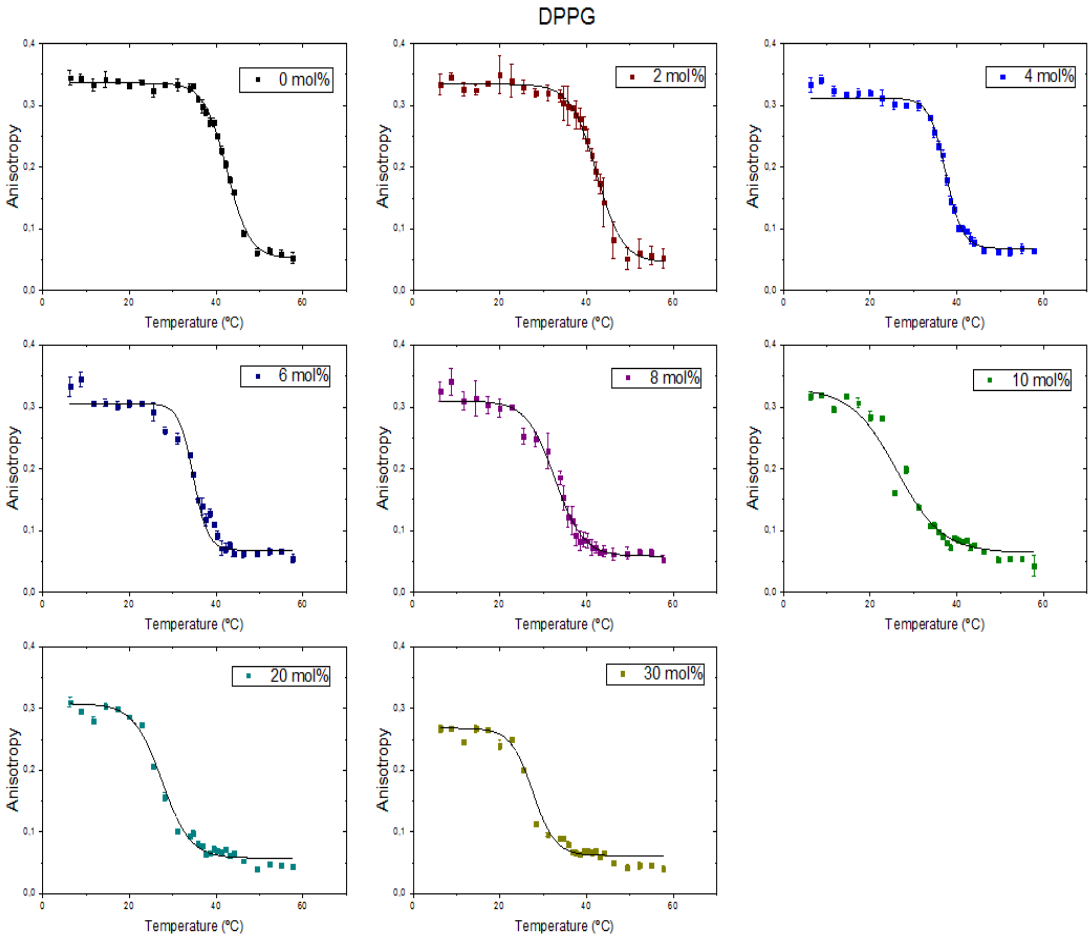

Figure 3.10: Anisotropy versus temperature (ºC) as [C_{14}MIM][Cl] is add to DPPG at 0.5mM. The lines are purely to guide the eyes and have no physical meaning.

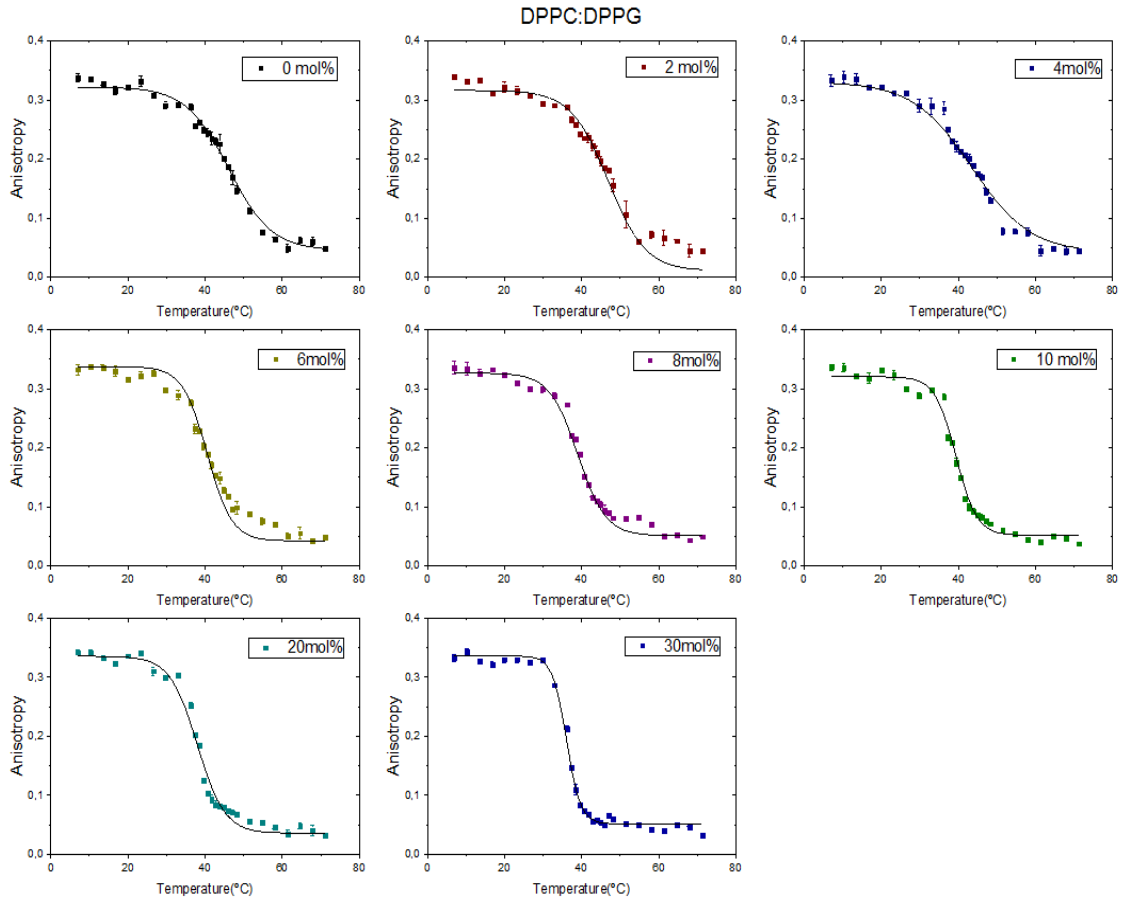

Figure 3.11: Anisotropy versus temperature (ºC) as [C_{14}MIM][Cl] is add to DPPC:DPPG at 0,5mM. The lines are purely to guide the eyes and have no physical meaning.

For DPPC:DPPG (Figure 3.11), the melting temperature decreased from 42.25±*0.13*ºC to 34.14ºC and for DPPG, the decay was more intense, from 42.5ºC to 25.25ºC. So, as in ζ-potential, the interaction of [C_{14}MIM][Cl] was higher with the negative vesicles as we can see in Figure 3.10 and Figure 3.11.

Figure 3.12 shows clearly the decay of the melting temperature as the amount of [C_{14}MIM][Cl] increases.

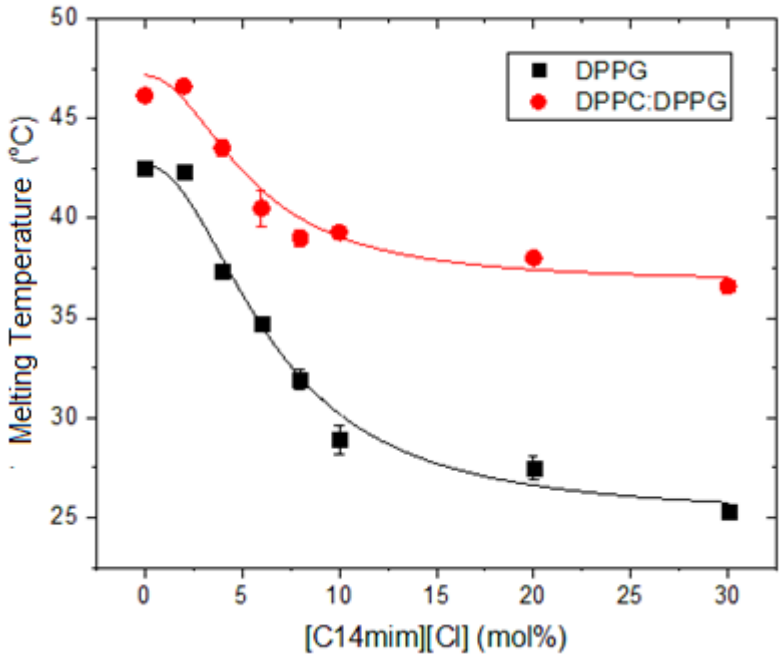

Figure 3.12: Melting temperature variation as function of [C_{14}MIM][Cl] concentration for DPPG and DPPC:DPPG. The lines are purely to guide the eyes and have no physical meaning.

It is noticeable for liposomes with negative charge (DPPG present) the LI is able to destabilize the lipid membrane and reduce the melting temperature (Table 3. 2). This can be evidence that the IL get into the lipids and "disorganize" the inner bilayer structure.

In Table 3. 2 the melting temperatures are shown for each biomimetic systems investigated as the amount of IL increases. The first three columns represent the zwitterionic vesicles and the last two the anionic vesicles.

[C_{14}MIM][Cl] (mol%)	DPPC (ºC)	DMPC (ºC)	DPPC:DMPC (ºC)	DPPC:DPPG (ºC)	DPPG (ºC)
0	*38.03±0.19*	*25.75±0.16*	*34.60±0.40*	*42.50±0.13*	*46.12±0.22*
2	-	-	-	*42.34±0.30*	*46.62±0.25*
4	-	-	-	*37.40±0.20*	*43.52±0.49*
6	-	-	-	*34.70±0.10*	*40.53±0.90*
8	-	-	-	*31.89±0.50*	*39.05±0.43*
10	*37.10±0.47*	*28.28±0.13*	*34.54±0.13*	*28.90±0.74*	*39.30±0.16*

20	*39.23±1.06*	*27.50±0.29*	*35.32±0.26*	*27.50±0.59*	*38.00±0.33*
30	*38.92±0.20*	*27.00±0.20*	*34.14±0.32*	*25.27±0.33*	*36.6±0.38*

Table 3. 2: Gel-fluid melting temperature in ^{o}C, increasing the amount of [C_{14}MIM][Cl].

In the bilayer, the hydrocarbon chains of the phospholipids influence each other by Van der Waals interactions (BLUME, 1993; CEVC; MARSH, 1987). The IL troubles the ordered gel stated of the bilayer and the anisotropy value decays faster. Antagonistically to the ζ-potential results, the IL did not changed significantly systems with DPPC.

3.4 Dynamic Light Scattering

Given the previous results, evidently the IL is capable of interacting with the lipid bilayer. To ensure [C_{14}MIM][Cl] embody or not in the bilayer, we measured the liposomes size after the addition of the IL in solution. If the IL incorporates into the lipid membrane the ratio of the liposomes may increase.

For zwitterionic vesicles composed by DPPC, DMPC, POPC I the absence and presence of sphingomyelin and cholesterol, there is no significant change on size. Figure 3.13 represents the mean vesicles diameter after the addition of [C_{14}MIM][Cl] at final concentration of 30 mol% (0.3mM). Here, we made sure to use concentrations of IL under the CMC (critical micellar concentration) to assure the [C_{14}MIM][Cl] would not form micelles in solution.

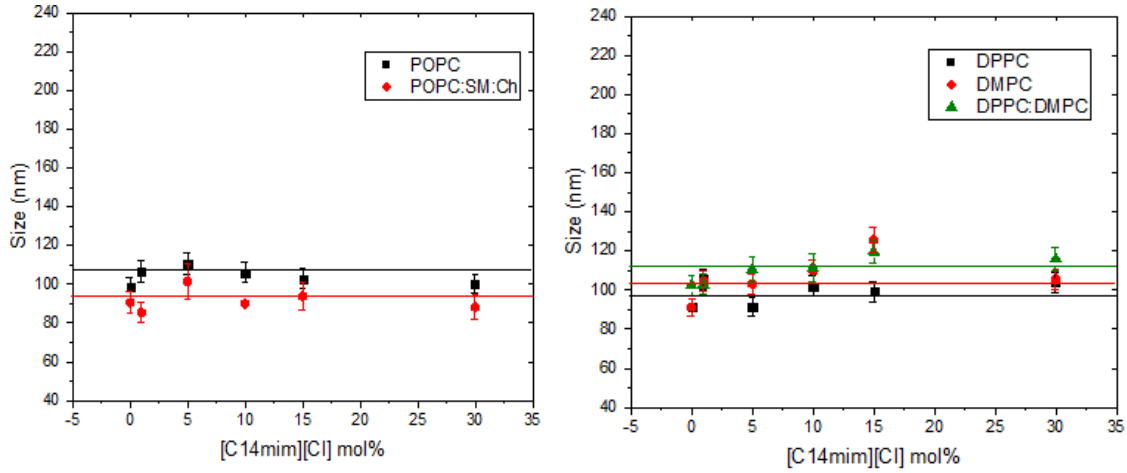

Figure 3.13: Particle mean size in nm of POPC and POPC:SM:Ch (1:1:1) on the left and DPPC, DPPC:DMPC (1:1) and DMPC by the addition of [C_{14}MIM][Cl].

As showed before, the IL has smaller influence on zwitterionic lipid vesicles comparing to the negative liposomes because of its positive charge. For DPPC, the gel-fluid melting temperature does not have a significant change, showing that IL does modify the local microviscosity. This is coherent with the uniformity of the diameter in Figure 3.13.

In contrast, both DPPG and DPPC:DPPG liposomes showed large size variation as IL concentration increases (

Figure 3.14). For DPPG, the diameter of the vesicle increased from 84±1nm to 176±1nm in the presence of 30 mol% pf [$C14_{MIM}$][Cl], whereas for DPPC:DPPG it increases from 95±1nm to 196±1nm.

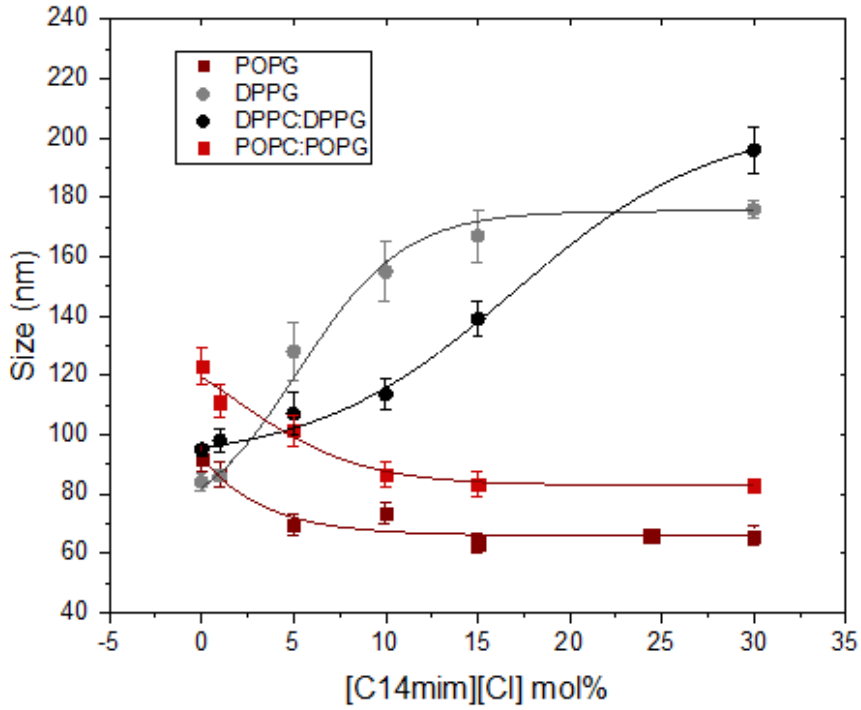

Figure 3.14: Particle mean size in nm of POPG, POPC:POPG (1:1), DPPG and DPPC:DPPG (1:1) by different concentrations of [C_{14}MIM][Cl].

On the other hand, vesicles composed by 1-palmitoyl-2-oleoyl alcyl chain lipids did not raised their size as the dipalmitoyl lipids did. Instead, POPG and POPC:POPG vesicles got smaller (

Figure 3.14). POPG liposomes diminished from 92±1nm to 66±1nm and POPC:POPG from 123±1nm to 83±1nm.

In contrast, both DPPG and DPPC:DPPG vesicles showed great change in the melting temperature and diameter as a function of the IL concentration. Thus, this increase in size is attributable to the incorporation of the IL into the vesicles. This is a surfactant-like behavior-like in agreement with other authors (LÓPEZ et al., 1998; PATERNOSTRE et al., 1995; POLOZOVA et al., 1995).

Table 3. 3 shows all PdI values listed by the IL concentration variation. Noteworthy, in all studied cases these values were <0.7, indication the the cumulant analysis can be applied.

	DPPC	DMPC	DPPG	POPC	POPG	POPC:POPG	DPPC:DPPG	DPPC:DMPC
0 mol%	0.125	0.062	0.158	0.11	0.095	0.099	0.101	0.02
1 mol%	0.113	0.088	0.134	0.132	0.097	0.102	0.311	0.227
5 mol%	0.137	0.122	0.298	0.115	0.096	0.119	0.178	0.46
10 mol%	0.122	0.204	0.104	0.105	0.099	0.077	0.105	0.482
15 mol%	0.365	0.119	0.025	0.131	0.103	0.082	0.053	0.374
30 mol%	0.391	0.175	-	-	-	-	0.057	0.251

Table 3. 3: PdI valeus according to the lipid ans the concentration of IL.

For POPC and POPG there was no significant variance in PdI values. However, concerning DPPC and DMPC PdI doubled in the presence of high IL amount. This behavior is probably due to the charge shielding that occurs as the IL is added. However, even with some fluctuation, PdI values do not exceed 0.7 and the cumulant analysis appropriate.

3.5 Small Angles X-ray scattering

As a complementary tool to the DLS results SAXS measurements were performed. Making use of the software Genfit, developed by Prof. Francesco Spinozzi (SPINOZZI et al., 2014), the best fitting for the experimental scattering curves provides the best fitting parameters. The parameters support information on the bilayer inner structure as well as the electronic density and the size of the polar head, the acyl chain and the methyl (SPINOZZI et al., 2014). Using the fitting parameters, we were able to map the electronic density profile. Here, we made sure to use concentrations of IL under the CMC (critical micellar concentration) to assure the [C_{14}MIM][Cl] would not form micelles in solution.

We used concentrations of IL smaller than the CMC (critical micellar concentration) to assure the $[C_{14}MIM][Cl]$ would not form their own micellar structures. One should bear in mind however, that the presence of vesicles could decrease significantly the CMC value of the IL, meaning lipid aggregation. Lipids experimental intensity are presented followed by the correspondent electronic density profile.

Figure 3.15 shows the SAXS curves of LUV composed by DPPC in the absence and presence of $[C_{14}MIM][Cl]$ at 15, 30 and 45 mol%. The curves are typical of the scattering from unilamellar vesicles, with a broad peak at q ~0.11 $Å^{-1}$ (FERNANDEZ et al., 2008) ievidences a core-shell structure, as expected. As one can see, the theoretical model described in section 2.2.5 (solid line in Figure 3.15) is a good fitting of the bilayer structural model. The addition of increasing amount of $[C_{14}MIM][Cl]$ does not affect significantly the bilayer scattering profile.

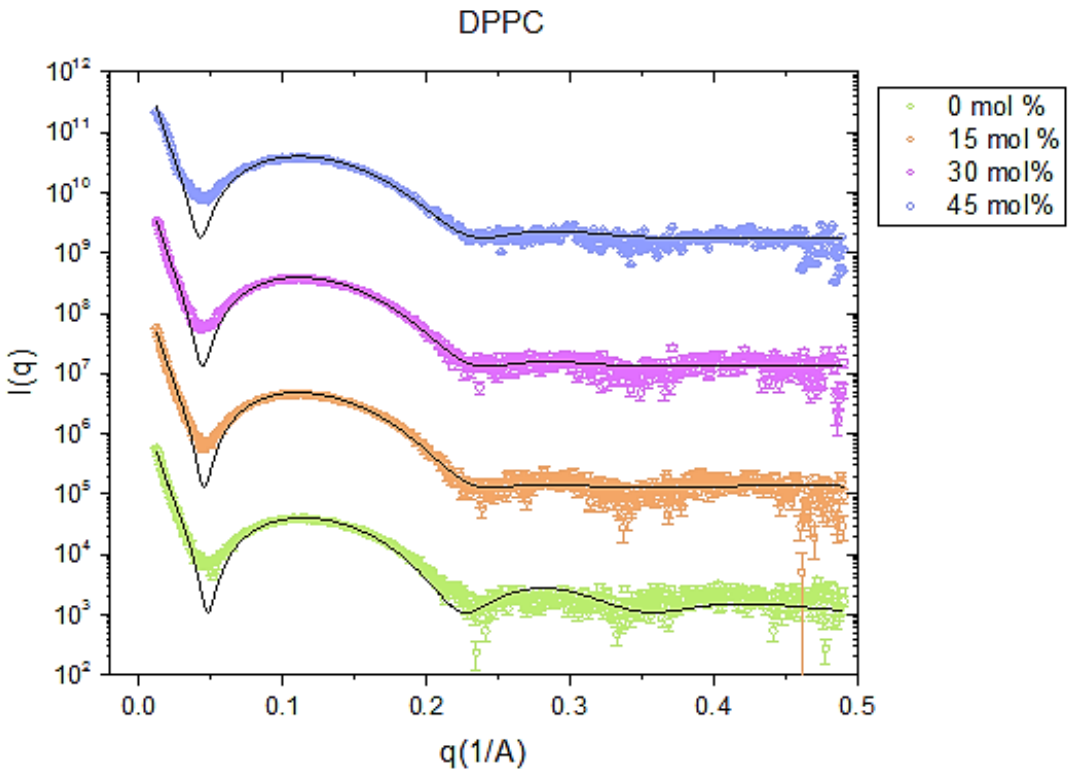

Figure 3.15: SAXS curves for DPPC with 0, 15, 30 and 45 mol% of [C_{14}MIM][Cl]. The solid lines represent the best fitting as described in 2.2.5.

The fitting parameters are presented in Table 3. 4 and reveal that the addition of the IL does not alter significantly the main features of the hydrophobic environment of the zwitterionic membrane. Actually, it increases the polar head thickness from 11.1±0.6 Å to 18.0±0.7 Å in the presence of 15 mol% of [C_{14}MIM][Cl] (Figure 3.16).

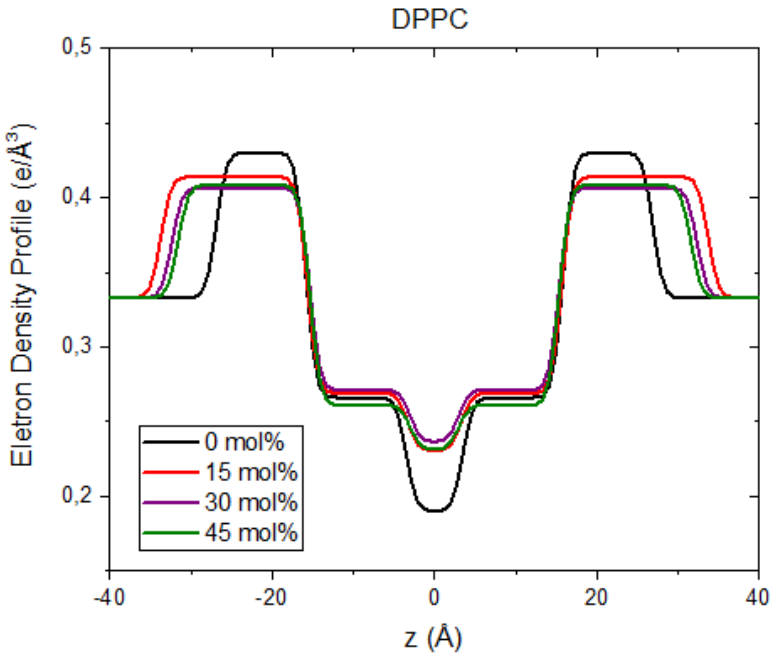

Figure 3.16: Electronic density of DDPC as IL addition.

Therefore, the IL must reside close to the polar head region of the lipid membrane, without affecting significantly the inner region of the bilayer. This can be correlated with the previous results of DLS and ζ-potential, which is evident that the IL is capable of interacting with the lipid bilayer, but for the vesicles composed by DPPC, there is no significant change on the size and the local microviscosity.

Systems composed by the negatively charged lipid DPPG, up to 30 mol% there is a tendency of softening the curve. However, there is no change on the unilamellar profile and the fitting is good (Figure 3.17).

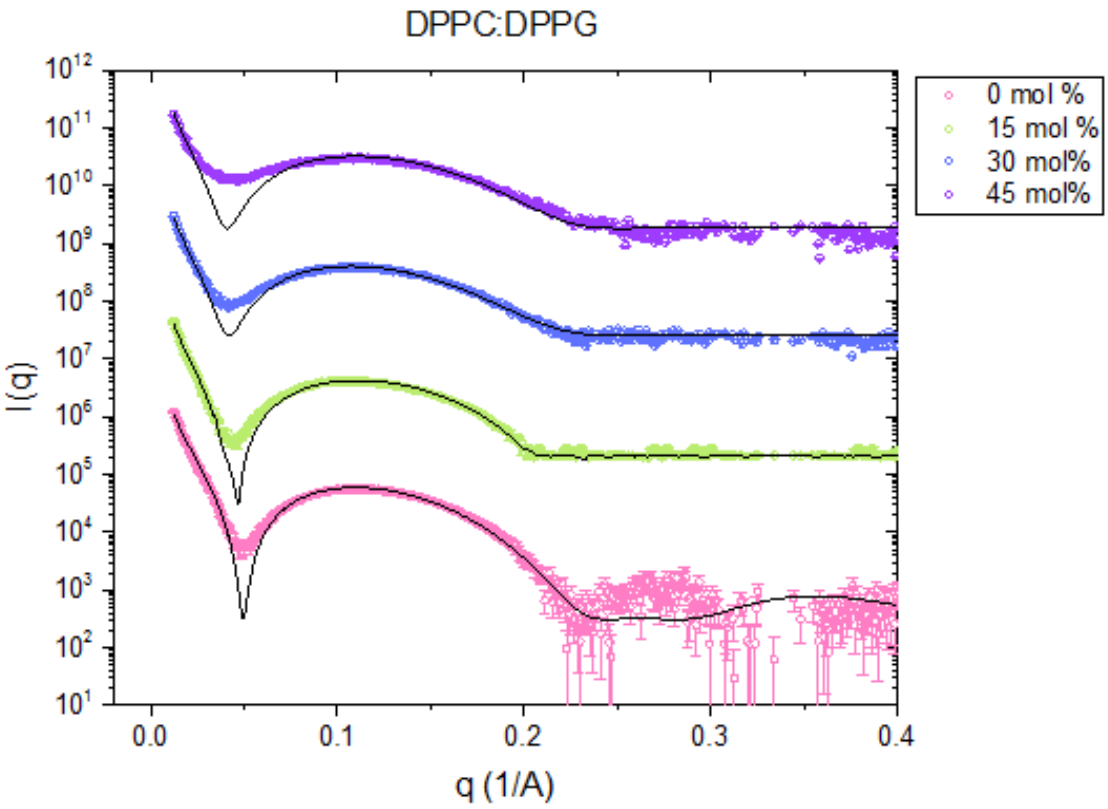

Figure 3.17: SAXS curves for DPPC:DPPG with 0, 15, 30 and 45 mol% of [C_{14}MIM][Cl]. The lines represent the best fitting as described in 2.2.5.

As can be seen in Table 3. 4, the fitting parameters for DPPC:DPPG reveal that the addition of IL alter the hydrophobic environment of the membrane by increasing the polar head thickness from 9.3±0.6 Å to 17.8±0.8 Å in the presence of 45 mol% of [C_{14}MIM][Cl]. The polar electron density raised from 0.380±0.004 (e/Å^3) to 0.440±0.008 (e/Å^3) in the presence of 45 mol% of [C_{14}MIM][Cl] (Figure 3.18).

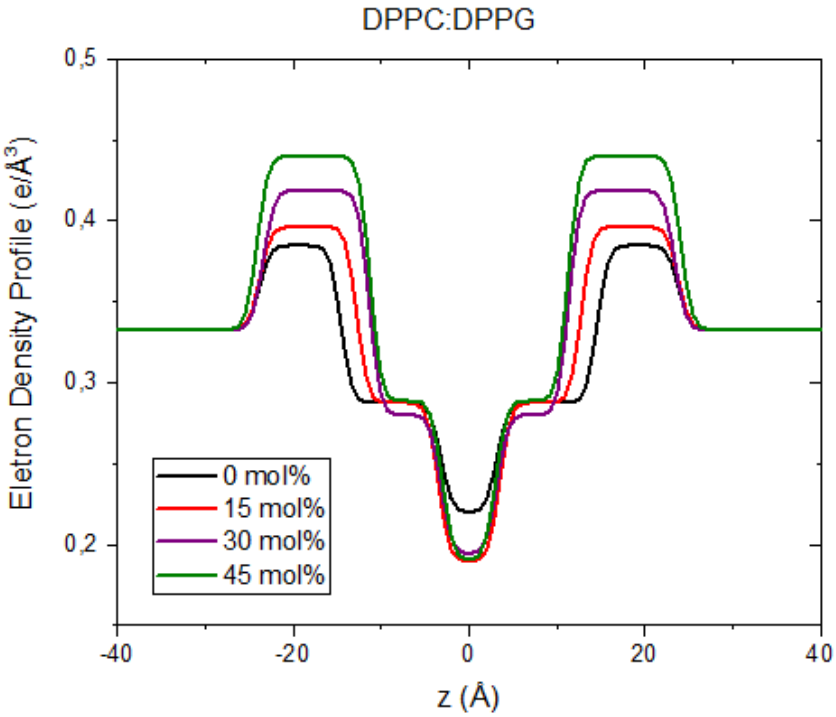

Figure 3.18: Electronic density of DDPC:DPPG as the IL is added.

The methyl length and the eletronic density values decreased from 3.2±0.3 Å to 3.1±0.2 Å and 0.220±0.007 (e/Å^3) to 0.19±0.01 (e/Å^3) as 45 mol% of IL is added, respectivly. Also the acyl chain length declined from 11.4±0.4 Å to 8.2±0.5 Å, showing the IL indeed incorporates into the bilayer.

For DPPG the experimental scattering curve flattening is evident (Figure 3.19).

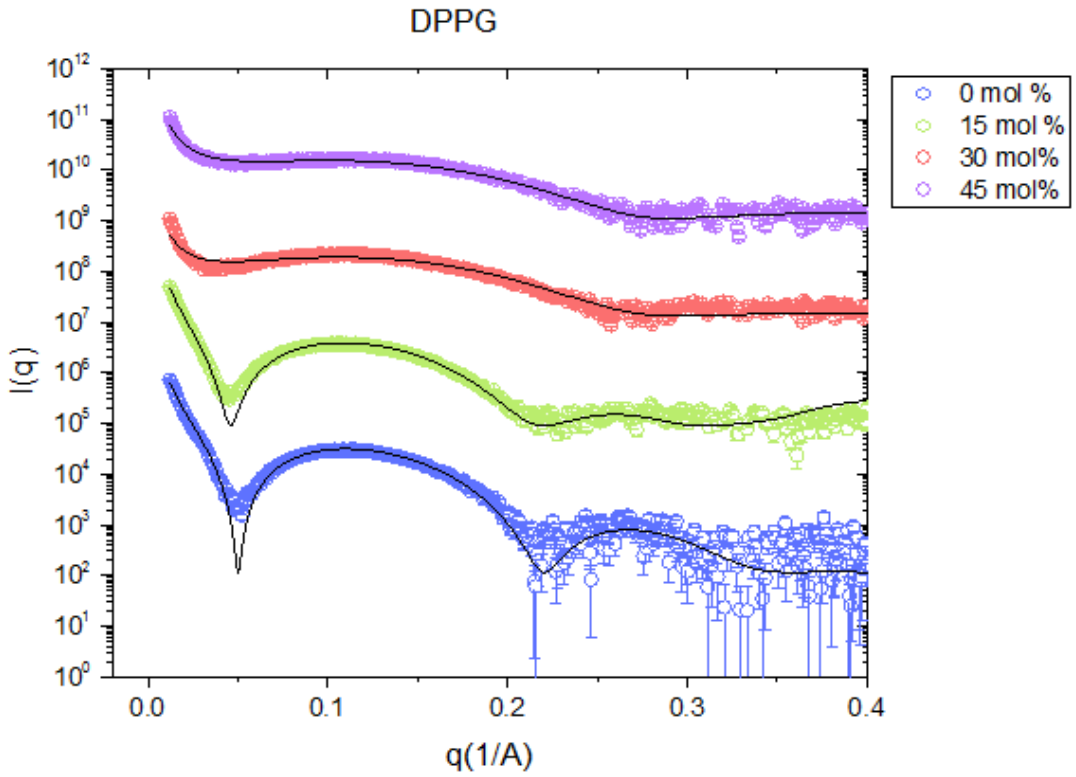

Figure 3.19: SAXS curves for DPPG with 0, 15, 30 and 45 mol% of [C_{14}MIM][Cl]. The lines represent the best fitting as described in 2.2.5.

Simillary to DPPC:DPPG, polar head and acyl chain length values changes as the IL is added in the systems. Also the polar head electron density decreases (Figure 3.20).

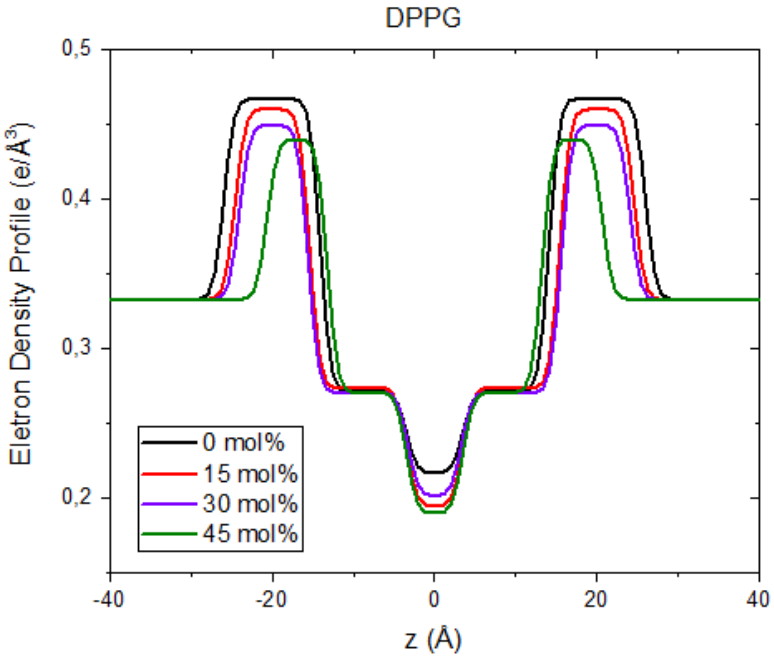

Figure 3.20: Electronic density of DDPG as the IL is added.

Polar head group length decreased from 11.9±0.2 Å to 7.4±0.9 Å and electron density from 0.470±0.002 (e/Å^3) to 0.440±0.006 (e/Å^3) in the absence and presence of 45mol% of IL, which means that the IL must reside in the membrane near the polar/apolar interface. Since the acyl chain length increases from 10.59 Å to 13.71 Å, it can be an evidence that the IL incorporate the bilayer and alter the hydrophobic CH_2 tail.

Fitting parameters obtained for the lipid systems composed of DPPC, DPPC:DPPG or DPPG are shown in Table 3. 4.

DPPC				
[C_{14}MIM][Cl] (mol%)	**0**	**15**	**30**	**45**
R_{pol} (Å)	11.1±0.6	18.0±0.7	17.0±0.9	15.3±0.9
R_{par} (Å)	12.4±0.5	8.2±0.4	9.1±0.6	9.8±0.5
R_{CH3} (Å)	3.5±0.2	3.3±0.3	3.0±0.3	3.2±0.1
ρ_{pol} (e/Å^3)	0.490±0.003	0.410±0.006	0.410±0.006	0.440±0.004
ρ_{par} (e/Å^3)	0.290±0.004	0.260±0.003	0.270±0.004	0.260±0.003
ρ_{CH3} (e/Å^3)	0.190±0.007	0.230±0.005	0.240±0.004	0.200±0.008
DPPC:DPPG				
[C_{14}MIM][Cl] (mol%)	**0**	**15**	**30**	**45**
R_{pol} (Å)	9.3±0.6	17.0±0.8	19.1±0.5	17.8±0.2
R_{par} (Å)	11.4±0.4	9.3±0.4	8.1±0.3	8.2±0.5
R_{CH3} (Å)	3.2±0.3	3.5±0.5	3.2±0.3	3.1±0.2
ρ_{pol} (e/Å^3)	0.380±0.004	0.400±0.007	0.420±0.003	0.440±0.008
ρ_{par} (e/Å^3)	0.290±0.003	0.290±0.008	0.280±0.004	0.290±0.006
ρ_{CH3} (e/Å^3)	0.220±0.007	0.190±0.008	0.190±0.004	0.19±0.01
DPPG				
[C_{14}MIM][Cl] (mol%)	**0**	**15**	**30**	**45**
R_{pol} (Å)	11.9±0.2	9.2±0.3	8.5±0.6	7.4±0.9
R_{par} (Å)	10.6±0.2	11.9±0.2	13.0±0.4	13.7±0.5
R_{CH3} (Å)	3.5±0.1	3.5±0.1	3.4±0.3	3.5±0.3
ρ_{pol} (e/Å^3)	0.470±0.002	0.460±0.003	0.450±0.004	0.440±0.006
ρ_{par} (e/Å^3)	0.270±0.001	0.270±0.002	0.270±0.008	0.270±0.005
ρ_{CH3} (e/Å^3)	0.220±0.003	0.190±0.004	0.230±0.007	0.190±0.008

Table 3. 4: Fitting parameters obtained for the lipid systems composed of DPPC, DPPC:DPPG (1:1) or DPPG, increasing the amount of [C14MIM][Cl]. Rpar CH2 chain length, RCH3 methyl length Rpol polar head thickness, ρpar, ρCH3 and ρpol respective electron

3.6 Optical Microscopy

To elucidate the effect of the [$C14_{MIM}$][Cl], we studied its effect, by means of optical microscopy, on Giant Unilamelar Vesicles (GUVs) for three different systems: 100 mol% POPC, 80:20 POPC:POPG and 50:50 POPC:POPG in absence and presence of 1.33mM and 2.33mM of [C_{14}MIM][Cl]. To guarantee that we were able to visualize the beginning of the IL/GUV interaction, we first isolated one GUV, and then added IL. The first attempts failed because IL addition caused influx, moving the GUV away from the focus region, making impossible to follow the same GUV and control the beginning of their interaction. Moreover, in some cases GUVs were already destroyed when isolated (what took around 1.5 minutes). To solve this problem, we added a small volume of IL (< 4μl of a ~1mM stock solution) per time. This amount of volume did not cause inflow. Consequently, the period to start interaction was longer than compared to first attempts, but we were able to follow the same GUV during the experiment. Here, we made sure to use concentrations of IL under the CMC (critical micellar concentration) to assure the [C_{14}MIM][Cl] would not form micelles in solution.

Experiments were recorded at 10 pps (photos per second). The movies resulted in photo sequences and the relevant ones were shown here. It is important to emphasize that the photos showed here represent the most frequent effects of all experiments, nevertheless, qualitative results are important to infer the IL action in the vesicles.

Figure 3.21 there is the first series of photos of 100mol% POPC with 1.33mM. IL effect was similar to all studied concentrations tested.

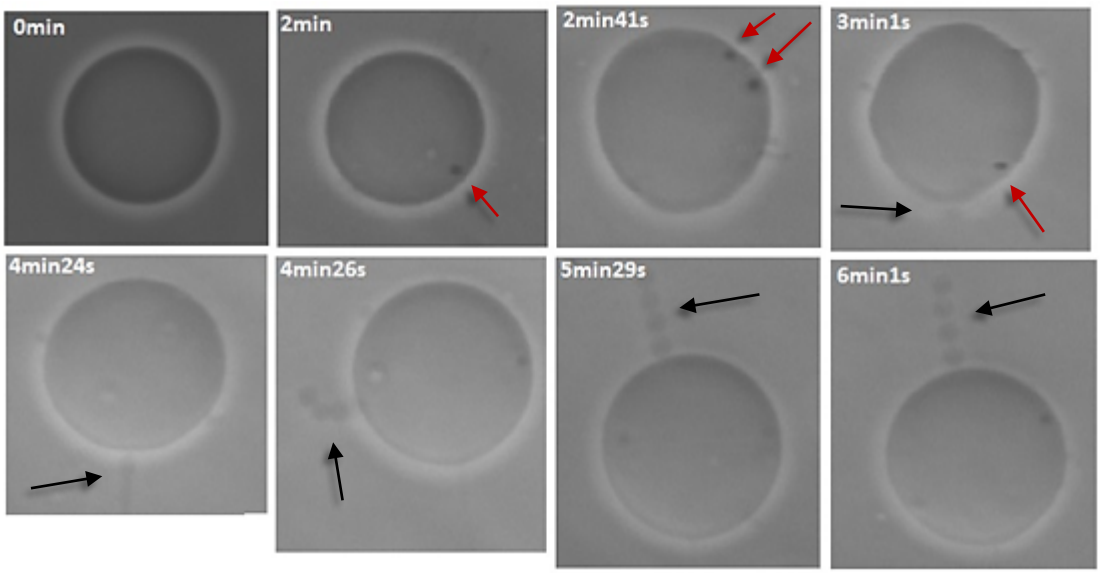

Figure 3.21: GUVs composed of 100 mol% POPC under the effect of 1.33mM of [C_{14}MIM][Cl].

Initially, liposomes area increases, which was evidenced by an increase in the fluctuation of the lipid bilayer, meaning that the IL incorporates into the bilayer. Small black dots represents regions with probably both IL and lipids (red arrows). Subsequently, *buds* (small vesicles that stays connected to the main vesicle) are also formed (black arrows). Buds formation is an essential initial step in releasing the excess of area to maintain the spherical shape for the vesicles (BELAY; CHUN IL; SCHIAVONE, 2016). Afterward, optical contrast decreases, probably due to pores formation in the membrane, or to some lipid re-arrangement that allowed the inter-change between the inner and outer regions of the GUV.

Figure 3.22 shows the sequence of images of 100 mol% POPC in presence of 2.33mM of IL. Again, the final image represents buds formation; however, it took a smaller period to acquire, around half the period of 1.33mM.

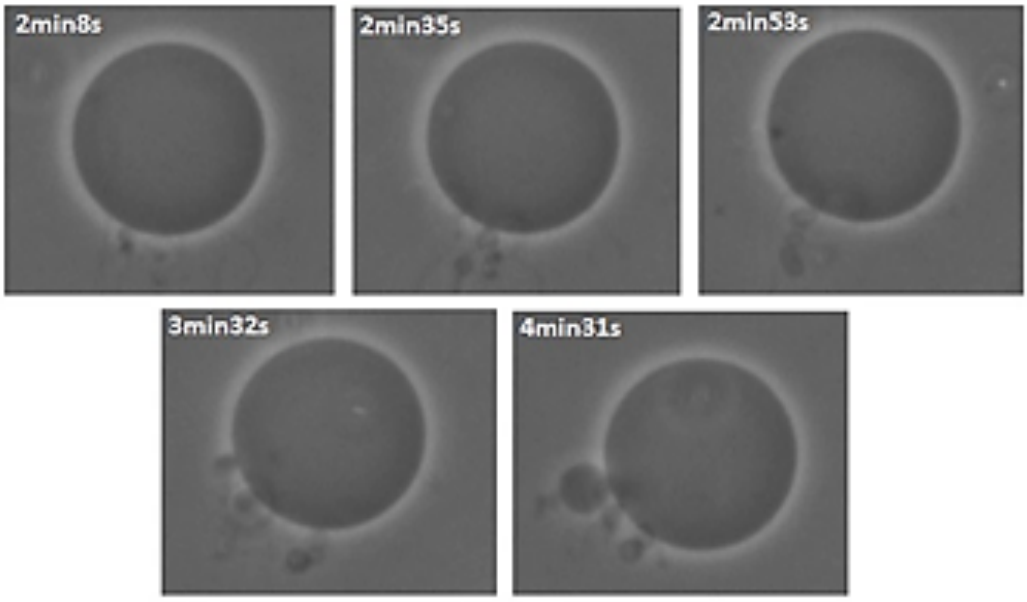

Figure 3.22: GUVs composed of 100 mol% POPC under the effect of 2.33mM of [C_{14}MIM][Cl].

For negative vesicles, we can also observe the IL/lipids interaction and increase of area, followed by vesicle destruction. For 80:20 POPC:POPG, the same amount of IL was added. In Figure 3.23, 1.33 mM of [C_{14}MIM][Cl] is added and after 9 minutes and 1 second, the vesicle is destroyed by the presence of IL.

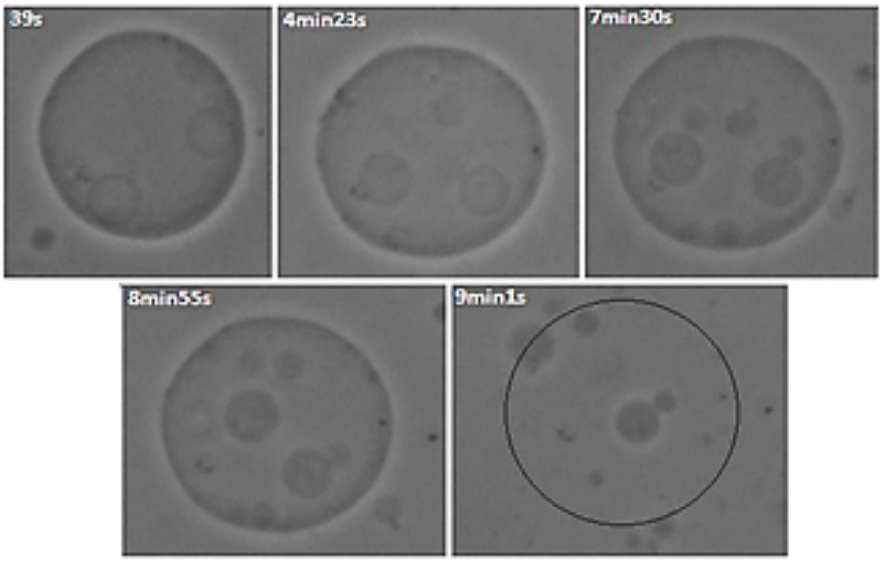

Figure 3.23: GUVs composed of 80:20 POPC:POPG under the effect of 1.33mM of [C_{14}MIM][Cl]. The black circle represents que vesicle disrupted.

As we increased IL concentration to 2.33mM, the effects on the GUVs were evidenced in smaller period of time. In Figure 3.24, we can notice the disruption of almost all vesicles present in the photo. Here there is also the increase of vesicles area. Interaction was faster as compared to 1.33mM; it took 4 minutes and 49 second to the disruption of the first vesicle.

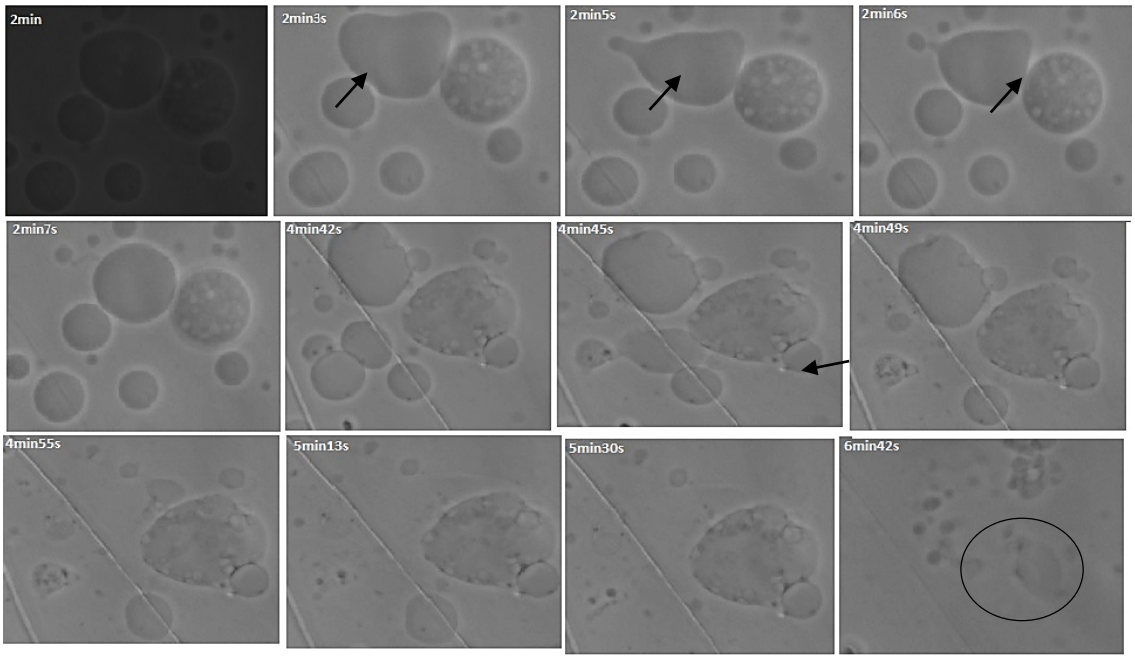

Figure 3.24: GUVs composed of 80:20 POPC:POPG under the effect of 2.33mM of [C_{14}MIM][Cl]. The black circle represents que vesicle disrupted.

When the amount of negatively charged lipid POPG increases in the system, the membrane destabilization happens likewise. In the presence of 1.33mM of [C_{14}MIM][Cl] interacting with POPC:POPG 50:50 (Figure 3.25), a similar behavior was observed, i.e., increased vesicle area followed by membrane solubilization.

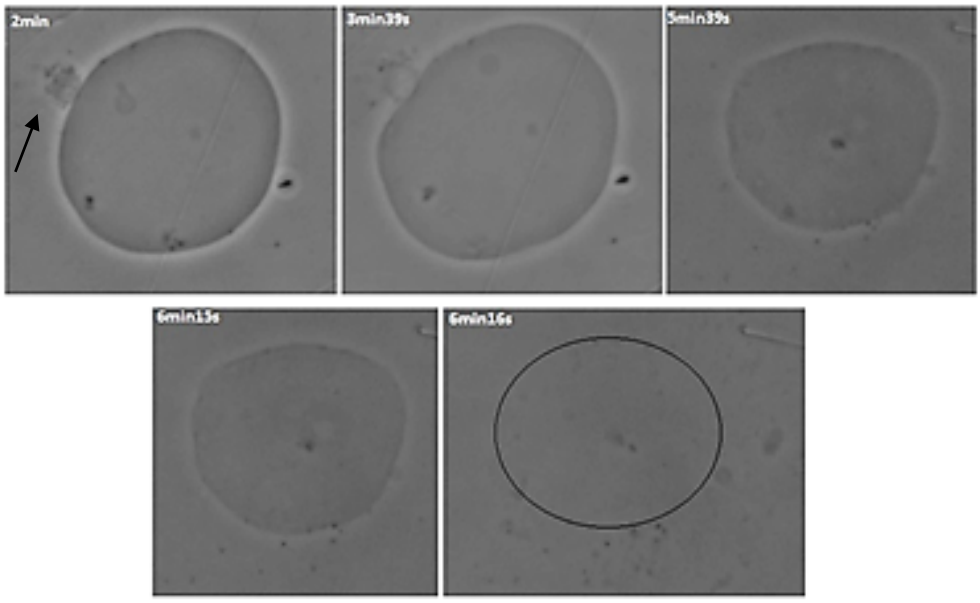

Figure 3.25: GUVs composed of 50:50 POPC:POPG under the effect of 1.33mM of [C_{14}MIM][Cl]. The black circle represents que vesicle disrupted.

For 2.33 mol% (Figure 3.26), it is possible to observe the IL/lipids interaction by buds formation and loss of optical contrast followed by the disruption of the liposome, similar to the other systems. After 5 minutes and 23 second, the vesicle is destroyed by the presence of IL.

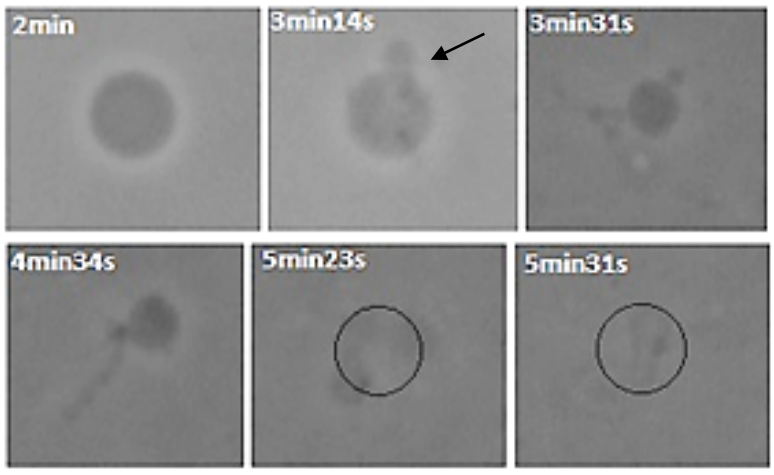

Figure 3.26: GUVs composed of 50:50 POPC:POPG under the effect of 2.33mM of [C_{14}MIM][Cl]. The black circle represents que vesicle disrupted.

According to the experiments, we propose that [C_{14}MIM][Cl] incorporates into the GUV, in agreement with other studied from the literature (ARCHILHA, 2009; MATTEI; FRANÇA; RISKE, 2015; MATTEI et al., 2017).

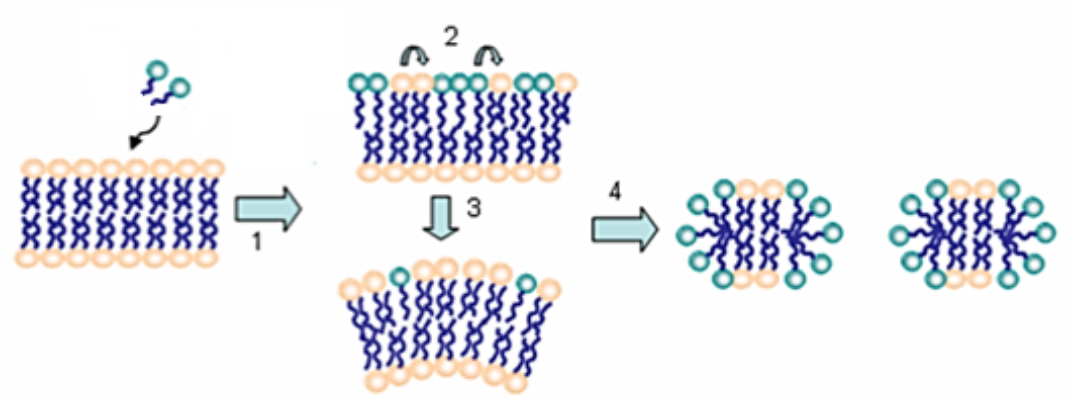

Figure 3.27: IL incorporation into the bilayer, where the green molecules are the IL and the orange molecules are the lipids. Adapted from (ARCHILHA, 2009)**.**

Because of IL accumulation, the bilayer curves to accommodate the IL. The membrane do not stand the asymmetry between the layers and it will tend to form micelles, consequently, pores and buds (Figure 3.27). Therefore, [C_{14}MIM][Cl] action in the bilayer can be compared to surfactant behave as interact to vesicles, as shown in previous studies (BELAY; KIM; SCHIAVONE, 2016; LICHTENBERG; AHYAYAUCH; GOÑI, 2013; SHINODA; DEVANE; KLEIN, 2010).

4. Concluding comments

In this work, the influence of the ionic liquid [C_{14}MIM][Cl] in model membranes of DPPC, POPC, DPPC:DPPG, POPC:POPG (1:1), DPPG and POPG were systematically investigated in other to better understand how model membranes endure changes among exposure to ILs. To do so we took hand of zeta potential, DLS, optical microscopy, surface tension, SAXS and anisotropy measurements.

First, we obtained ζ-potential measurements as key indicator of superficial charge of the liposomes. The results indicated the IL changes the superficial charge of the liposomes (zwitterionic and negatively charged), increasing the ζ-potential value. This indicates the IL interact, at least, superficially with the vesicles. Therefore, to make sure if the interaction was superficial or not, the anisotropy value and the size was investigated.

We noticed that IL is also able to change the fluorescence anisotropy and, as consequence, the fluidity of the vesicles. The imidazolium-based ionic liquid weakened the interaction between the negatively charged lipid molecules. Consequently, as the amount of IL escalates, the melting temperature decreased and the size increased. While, for zwitterionic vesicles, no significant change in size and melting temperature was evidenced.

As a complementary tool to the DLS results we performed SAXS measurements. The electronic density and the size of the polar head parameters changes support the penetration of the [C_{14}MIM][Cl] into the bilayer structure. For the zwitterionic vesicles, the electronic density profile indicated that the IL

tends to reside on the polar head region, while for the anionic vesicles, the IL alter the hydrophobic environment. Qualitative results of optical microscopy were important to infer about IL action in the vesicles. [C_{14}MIM][Cl] incorporate into the GUV and stays, probably and initially, at the out layer of the membrane. However, with the IL accumulation, the membrane do not stand the asymmetry between the layers and form pores and buds.

We suggest the following model (Figure 4.1), where the ionic liquid penetrate into the lipid bilayers. However, for vesicles containing POPG or DPPG, the electrostatic interaction between the vesicles and the positive IL [C_{14}MIM][Cl] is stronger and more probable.

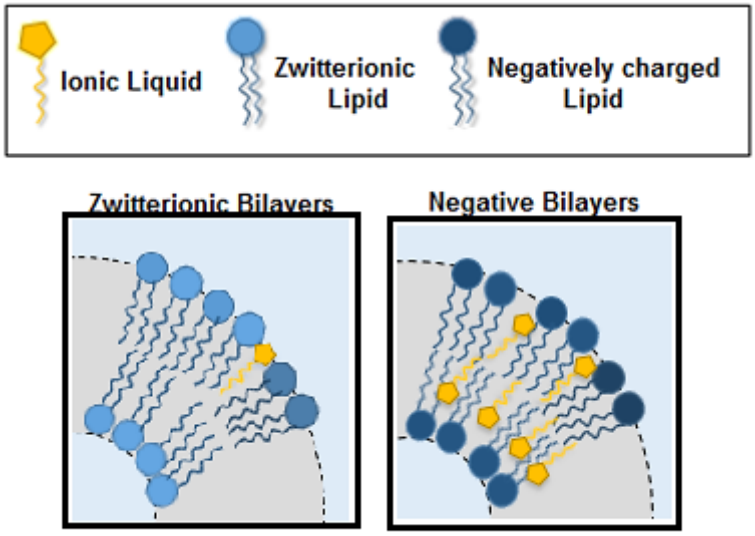

Figure 4.1: Interaction model between lipids and IL. For zwitterionic vesicles, the IL endure in the polar head region. For negatively charged vesicles, it incorporates into the bilayer.

Figure 4.1 show two scenarios. The zwitterionic bilayers, where the IL tend reside close to the polar head region without affecting significantly the inner region of the bilayer. And the negative bilayers that, by electrostatic interaction, increases in size and destabilize the vesicle.

5. References

AMELOOT, M. et al. Fluorescence anisotropy measurements in solution: Methods and reference materials (IUPAC Technical Report). **Pure & Applied …**, v. 85, n. 3, p. 589–608, 2013.

ANASTAS, P. T.; KIRCHHOFF, M. M. Origins, current status, and future challenges of green chemistry. **Accounts of Chemical Research**, v. 35, n. 9, p. 686–694, 2002.

ANDRICH, M. P.; VANDERKOOI, J. M. Temperature dependence of 1,6-diphenyl-1,3,5-hexatriene fluorescence in phophoslipid artificial membranes. **Biochemistry**, v. 15, n. 6, p. 1257–1261, 1976.

ARCHILHA, N. L. **Interação entre um peptídeo antimicrobiano e vesículas de fosfolipídeos**. [s.l: s.n.].

ATKIN, P.; PAULA, J. **Physical chemistry**. [s.l: s.n.].

BELAY, T.; CHUN IL, K.; SCHIAVONE, P. Mechanics of a lipid bilayer subjected to thickness distension and membrane budding. **Mathematics and Mechanics of Solids**, p. 1–18, 2016.

BELAY, T.; KIM, C. I.; SCHIAVONE, P. Bud formation of lipid membranes in response to the surface diffusion of transmembrane proteins and line tension. **Mathematics and Mechanics of Solids**, p. 1–17, 2016.

BERTHOD, A.; RUIZ-ÁNGEL, M. J.; CARDA-BROCH, S. **Ionic liquids in separation techniquesJournal of Chromatography A**, 2008.

BLEES, M. H. Foundations of Colloid Science. **Colloids and Surfaces A: Physicochemical and Engineering Aspects**, v. 210, n. 1, p. 125, 2002.

BLUME, A. **Phospholipids HandbookDynamic Properties**, 1993.

BOYLE, J. Lehninger principles of biochemistry (4th ed.): Nelson, D., and Cox, M. **Biochemistry and Molecular Biology Education**, v. 33, n. 1, p. 74–75, 2005.

BUTT, H.-J.; GRAF, K.; KAPPL, M. **Physics and Chemistry of Interfaces**. [s.l: s.n.].

CARDA-BROCH, S.; BERTHOD, A.; ARMSTRONG, D. W. Solvent properties of the 1-butyl-3-methylimidazolium hexafluorophosphate ionic liquid. **Analytical and Bioanalytical Chemistry**, v. 375, n. 2, p. 191–199, 2003.

CEVC, D.; MARSH, G. **Phospholipid bilayers: physical principles and models**. [s.l: s.n.].

CHEN, L.-J. et al. Temperature dependence of critical micelle concentration of polyoxyethylenated non-ionic surfactants. **Colloids Surf., A**, v. 135, p. 175–181, 1998.

CHIAPPE, C.; PIERACCINI, D. **Ionic liquids: Solvent properties and organic reactivityJournal of Physical Organic Chemistry**, 2005.

CHU, B.; HSIAO, B. S. **Small-angle X-ray scattering of polymersChemical Reviews**, 2001.

CLOGSTON, J. D.; PATRI, A. K. Zeta potential measurement. **Methods in molecular biology (Clifton, N.J.)**, v. 697, p. 63–70, 2011.

D M JAMESON. Gregorio Weber, 1916-1997: A Fluorescent Lifetime. **Biophysical Journal**, v. 75, p. 419–421, 1998.

DALTIN, D. **Tensoativos: química, propriedades e aplicações**. [s.l.] Blucher, 2011.

DESIMONE, J. M. Practical approaches to green solvents. **Science (New York, N.Y.)**, v. 297, n. 5582, p. 799–803, 2002.

DOMINGUES, M. M. et al. RBPI21 interacts with negative membranes endothermically promoting the formation of rigid multilamellar structures. **Biochimica et Biophysica Acta - Biomembranes**, v. 1828, n. 11, p. 2419–2427, 2013.

DOMÍNGUEZ, A. et al. Determination of Critical Micelle Concentration of Some Surfactants by Three Techniques. **Journal of Chemical Education**, v. 74, n. 10, p. 1227–1231, 1997.

EISBERG, R.; RESNICK, R.; BROWN, J. **Quantum physics of atoms, molecules, solids, nuclei, and particles**. [s.l: s.n.]. v. 39

ENCYCLOPEDIA BRITANNICA. Britannica Online Encyclopedia. **Encyclopædia Britannica**, p. 1–73, 2010.

ENDRES, F. et al. Physical chemistry of ionic liquids. **Physical Chemistry Chemical Physics**, v. 12, n. 8, p. 1648, 2010.

ERDMENGER, T. et al. Recent developments in the utilization of green solvents in polymer chemistry. **Chemical Society reviews**, v. 39, n. 8, p. 3317–33, 2010.

FEIGIN; SVERGUN, D. I. **Structure Analysis by Small-Angle X-Ray and Neutron Scattering**. [s.l: s.n.]. v. 40

FERNANDEZ, R. M. et al. Influence of salt on the structure of DMPG studied by SAXS and optical microscopy. **Biochimica et Biophysica Acta - Biomembranes**, v. 1778, n. 4, p. 907–916, 2008.

FILHO, P. L. O. **Estudo Estrutural e Termodinâmico de Sistemas Auto-Organizados : Micelas em Solução**. [s.l.] University of São Paulo, 2013.

GAL, N. et al. Membrane interactions of ionic liquids: Possible determinants for biological activity and toxicity. **Biochimica et Biophysica Acta - Biomembranes**, v. 1818, n. 12, p. 2967–2974, 2012.

HAYES, R. et al. How water dissolves in protic ionic liquids. **Angewandte Chemie - International Edition**, v. 51, n. 30, p. 7468–7471, 2012.

HUNTER, R. J. **Zeta Potential in Colloid Science: Principles and Applications**. [s.l: s.n.]. v. 8

ISRAELACHVILI, J. N. Intermolecular and surface forces: second edition. **Intermolecular and surface forces: revised third edition**, 1991.

JEONG, S. et al. Elucidation of molecular interactions between lipid membranes and ionic liquids using model cell membranes. **Soft Matter**, v. 8, n. 20, p. 5501, 2012.

KOTZ, J. C.; TREICHEL, P. M.; WEAVER, G. C. Química y Reactividad Química. In: **Química y Reactividad Química**. [s.l: s.n.]. p. 1292.

LAKOWICZ, J. R. **Principles of fluorescence spectroscopy**. [s.l: s.n.].

LEHNINGER, A. L. **Lehninger principles of biochemistry, Second Edition**. [s.l: s.n.].

LI, C.-J.; TROST, B. M. Green chemistry for chemical synthesis. **Proceedings of the National Academy of Sciences of the United States of America**, v. 105, n. 36, p. 13197–13202, 2008.

LICHTENBERG, D.; AHYAYAUCH, H.; GOÑI, F. M. The mechanism of detergent solubilization of lipid bilayers. **Biophysical Journal**, v. 105, n. 2, p. 289–299, 2013.

LÓPEZ, O. et al. Direct formation of mixed micelles in the solubilization of phospholipid liposomes by Triton X-100. **FEBS Letters**, v. 426, n. 3, p. 314–318, 1998.

ŁUCZAK, J. et al. **Self-organization of imidazolium ionic liquids in aqueous solutionColloids and Surfaces A: Physicochemical and Engineering Aspects**, 2008.

MARSALEK, R. Zeta Potential - Applications. **International Conference on Environment and Industrial Innovation**, v. 35, p. 15–19, 2012.

MATTEI, B. et al. Membrane permeabilization induced by Triton X-100: The role of membrane phase state and edge tension. **Chemistry and Physics of Lipids**, v. 202, p. 28–37, 2017.

MATTEI, B.; FRANÇA, A. D. C.; RISKE, K. A. Solubilization of binary lipid mixtures by the detergent triton X-100: The role of cholesterol. **Langmuir**, v. 31, n. 1, p. 378–386, 2015.

MISKOLCZY, Z. et al. Aggregation and micelle formation of ionic liquids in aqueous solution. **Chemical Physics Letters**, v. 400, n. 4-6, p. 296–300, 2004.

NANOCOMPOSIX. Zeta Potential Analysis of Nanoparticles. **Nanocomposix Publications**, p. 1–6, 2012.

PATERNOSTRE, M. et al. Partition coefficient of a surfactant between aggregates and solution: application to the micelle-vesicle transition of egg phosphatidylcholine and octyl beta-D-glucopyranoside. **Biophysical Journal**, v.

69, n. 6, p. 2476–2488, 1995.

PATRA, D. et al. Effect of curcumin on liposome: Curcumin as a molecular probe for monitoring interaction of ionic liquids with 1,2-dipalmitoyl-sn-glycero-3-phosphocholine liposome. **Photochemistry and Photobiology**, v. 88, n. 2, p. 317–327, 2012.

PAUL, B. K.; MOULIK, S. P. **Ionic Liquid-Based Surfactant Science: Formulation, Characterization, and Applications**. [s.l: s.n.].

PECORA, R. Dynamic light scattering from macromolecules. **Proceedings of SPIE**, v. 1884, p. 2–15, 1993.

PERETÓ, J. et al. Fundamentos de bioquímica. In: **Dinámica de proteínas**. [s.l: s.n.]. p. 72–96.

POLESKI, M. et al. Wetting of surfaces with ionic liquids. **Physicochemical Problems of Mineral Processing**, v. 49, n. 1, p. 277–286, 2013.

POLOZOVA, A. I. et al. Temperature-induced micellar-lamellar transformation in binary mixtures of saturated phosphatidylcholines with sodium cholate. **FEBS Letters**, v. 358, n. 1, p. 17–22, 1995.

RUBIM, R. L. **Estudo de interações entre membranas lipídicas por experimentos de SAXS : o efeito da composição**. [s.l: s.n.].

SALAGER, JEAN L, ANTON, R. **Metodos de medecion de la tension superfcial o interfacialUniversidad de los Andes**. [s.l: s.n.].

SAUER, B. B.; DIPAOLO, N. V. Surface tension and dynamic wetting on polymers using the Wihelmy method: Applications to high molecular weights and elevated temperatures. **Journal of Colloid And Interface Science**, v. 144, n. 2, p. 527–537, 1991.

SCHNABLEGGER, H.; SINGH, Y. The SAXS guide: getting acquainted with the principles. **Anton Paar**, p. 124, 2013.

SELL, P. - J; NEUMANN, A. W. The Surface Tension of Solids. **Angewandte Chemie International Edition in English**, v. 5, n. 3, p. 299–307, 1966.

SHINODA, W.; DEVANE, R.; KLEIN, M. L. Zwitterionic lipid assemblies: Molecular dynamics studies of monolayers, bilayers, and vesicles using a new coarse grain force field. **Journal of Physical Chemistry B**, v. 114, n. 20, p. 6836–6849, 2010.

SPINOZZI, F. et al. GENFIT: Software for the analysis of small-angle X-ray and neutron scattering data of macro-molecules in solution. **Journal of Applied Crystallography**, v. 47, n. 3, p. 1132–1139, 2014.

STRYER, L. **Biochemistry**. [s.l: s.n.].

TUNDO, P. et al. Synthetic pathways and processes in green chemistry. Introductory overview. **Pure and Applied Chemistry**, v. 72, n. 7, p. 1207–1228, 2000.

VENTURA, S. P. M. et al. Design of ionic liquids for lipase purification. **Journal of Chromatography B: Analytical Technologies in the Biomedical and Life Sciences**, v. 879, n. 26, p. 2679–2687, 2011.

VENTURA, S. P. M. et al. Concentration effect of hydrophilic ionic liquids on the enzymatic activity of Candida antarctica lipase B. **World journal of microbiology & biotechnology**, v. 28, n. 6, p. 2303–10, 2012.

WASSERSCHEID, P.; KEIM, W. Ionic Liquids—New “Solutions” for Transition Metal Catalysis. **Angewandte Chemie International Edition**, v. 39, n. 21, p. 3772–3789, 2000.

WATSON, H. Biological membranes. **Essays In Biochemistry**, v. 59, n. 10, p. 43–69, 2015.

YANG, Z.; PAN, W. **Ionic liquids: Green solvents for nonaqueous biocatalysisEnzyme and Microbial Technology**, 2005.

YU, H.; HO, T. D.; ANDERSON, J. L. **Ionic liquid and polymeric ionic liquid coatings in solid-phase microextractionTrAC - Trends in Analytical Chemistry**, 2013.

ZHENG, J. et al. Ionic liquid-enhanced solid state electrolyte interface (SEI) for lithium–sulfur batteries. **Journal of Materials Chemistry A**, v. 1, n. 29, p. 8464, 2013.

Appendices

Appendix A - Anisotropy control

Since IL has surfactant-like behavior, we tested [$C14_{MIM}$][Cl], Triton X-100 and SDS interacting with DPPG to know in which concentration (in mol%) that

the vesicles rupture. The fluorescence anisotropy profile is shown in Figure 0.1, Figure 0.2 and Figure 0.3.

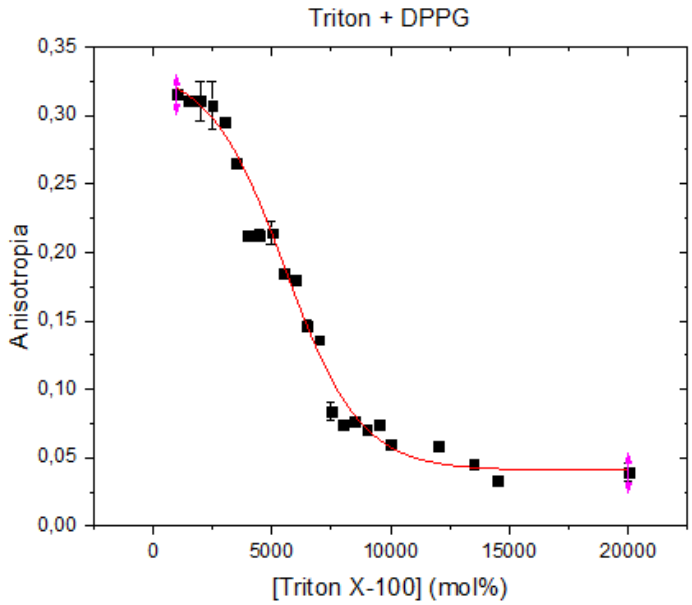

Figure 0.1: Triton X-100 interaction with DPPG vesicles.

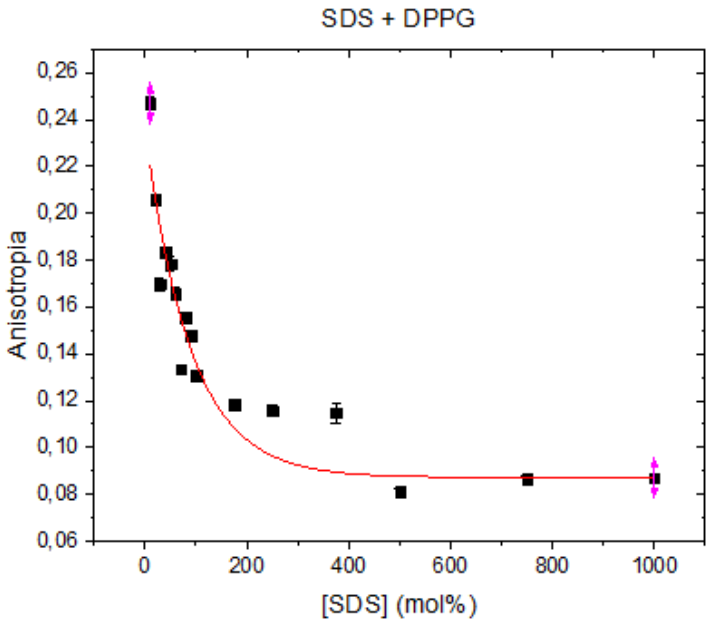

Figure 0.2: SDS interaction with DPPG vesicles

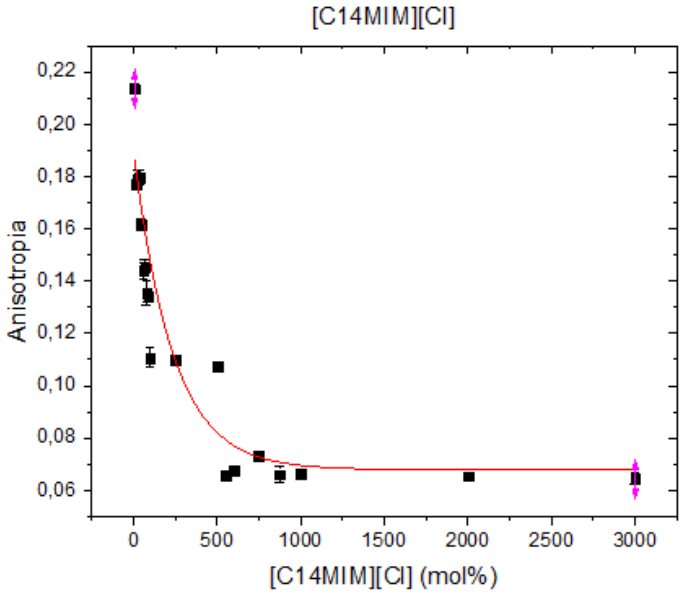

Figure 0.3: [$C14_{MIM}$][Cl] interaction with DPPG vesicles

For Triton X-100, above 10000 mol% it is possible that DPPG vesicles ruptures. For SDS above 200 mol% and for [C14 MIM][Cl] above 500 mol%.

All [$C14_{MIM}$][Cl] concentrations analyzed in this study were below 500 mol%, indicating that any change in fluorescence anisotropy by the addition of IL is due to the interaction between IL and vesicles.

Appendix B - Period of interaction between the IL and the vesicles.

To be sure about how long the IL takes to interact with vesicles, some tests were performed. Making use of the fluorimeter, first we measured the light intensity curve by the lipid sample with DPH and then added a small amount of [$C14_{mim}$][Cl] (0.15 mM in the final volume) and measured again with cycle mode by 30 times with 2 minutes intervals between them. In Figure 0.4, there is the DPPC and DPPG data for the first six times of the cycle mode. Since after the first six times the curves were the same, were ignored them for this plot.

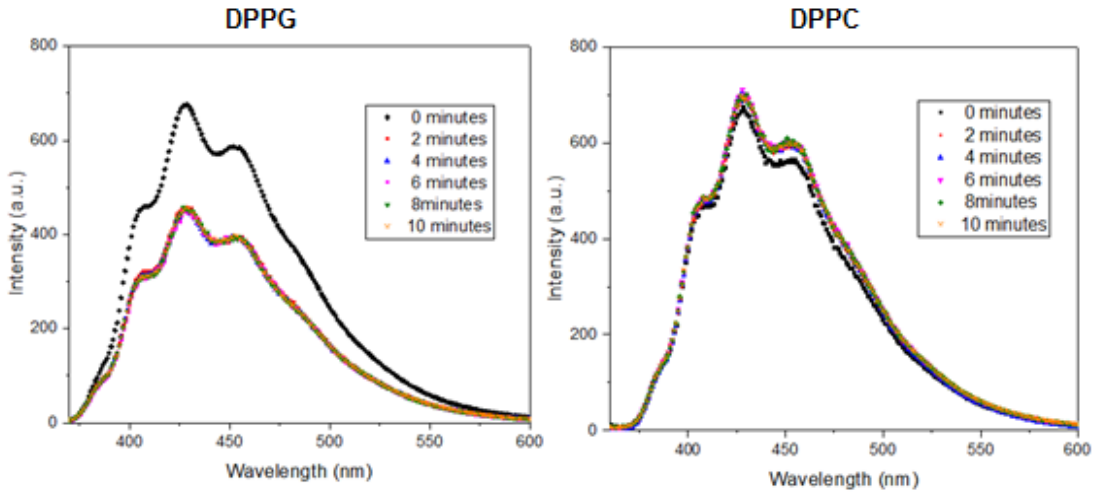

Figure 0.4: Fluorescence intensity of (a) DPPG and (b) DPPC with DPH in addition to a small amount of [$C14_{mim}$][Cl] (0.15 mM in the final volume). The black data is related to the vesicles without [$C14_{mim}$][Cl] and all the other represent measurements with cycle mode with 2 minutes intervals between them.

Between the first (without IL) and the second measurement (with IL) the Intensity profile are different, subtle for DPPC and greater for DPPG. However no difference between the second and the subsequent curves were detected. Indeed the curves overlap. This indicates the IL interaction with the membrane occur in less than 2 minutes. Such precaution was taken before all measures in this work.